Chemical Physics 599 (2025) 112890

Contents lists available at ScienceDirect

Chemical Physics

journal homepage: www.elsevier.com/locate/chemphys

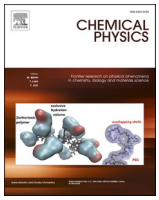

Natural plant extracts and phytochemicals as solar-cell sensitizers and UV protectors: Experimental and theoretical comparative assessments

Mohammed Madani Taouti [a], Ali Cheknane [a,*], Naceur Selmane [a,*], Noureddine Benaya [b], Hikmat S. Hilal [c,*]

[a] Laboratoire Matériaux, Systèmes Énergétiques, Énergies Renouvelables et gestion de l'Énergie (LMSEERGE), Université Amar Telidji de Laghouat, Bd des Martyrs BP37G, Laghouat 03000, Algeria
[b] Plateau technique d'analyse physico-chimique-laghouat-(PTAPC-L), Université Amar Telidji de Laghouat, Bd des Martyrs BP37G, Laghouat 03000, Algeria
[c] SSERL, Department of Chemistry, An-Najah National University, Nablus P400, Palestine

ARTICLE INFO

Keywords:
DSSC sensitizers & UV protectors
DFT/TDDFT & NBO analysis
Artemisia
Rosemary
Juniper
Haloxylon

ABSTRACT

Low-cost ecofriendly natural dyes are promising alternatives to synthetic metal-based counterparts in dye-sensitized solar cells. Extracts from North African *Artemisia campestris*, *Rosmarinus officinalis*, Haloxylon scoparium, and *Juniperus phoenicea* are comparatively evaluated here as future sensitizers and UV protectors. Experimentally, FTIR spectra confirm the presence of stable π-conjugations with -OH and -COOH groups necessary for good adsorption and charge transfer on TiO_2. Extract electronic-absorption spectra confirm broad absorption 190–800 nm, while TGA and DTA confirm stability. Corresponding phytochemical dyes, Esculetin-6-O-glucoside, Scutellarein, 3-(2-N-Acetyl-*N*-methylaminoethyl)indol, and 3-p-Coumaroylquinic acid are modeled using DFT/TDDFT (CAM-B3LYP/6-311G(d,p)) for their frontier orbital energies, light-harvesting efficiency (LHE), and charge-injection properties. Quercetin and Rutin are used for computational benchmarking. Natural-Bond-Orbital analysis correlates high intramolecular donor-acceptor stabilization and photovoltaic descriptors LHE and injection-driving force. Juniper- and Rosemary-derived compounds show UV-absorption and charge-transfer best performances, potentially promising sensitizers and UV-protectors. The results justify future device prototyping and natural dye optimization.

1. Introduction

Solar energy research is imperative [1]. Thus, new innovations in the field emerge to increase and enhance the supply of photovoltaics' generated electrical energy in the globe. One active research area is dye-sensitized solar cells (DSSCs), as possible replacement for conventional first-generation photovoltaics [2–4]. In DSSCs, dye molecules, anchored onto wide-bandgap semiconductor nanoparticles such as TiO_2, absorb in the visible region [5] in parallel to plants [6–9]. Various types of sensitizers for DSSCs were explored extensively. Effective synthetic metal complex dyes, explored by Graetzel et al. [2,10], often pose environmental concerns due to their heavy metal content [8,11]. Thus, researchers examined alternative metal-free synthetic dyes [12,13] with tunable properties and lower environmental impact [9]. However, metal-free synthetic dyes still need costly preparations. This turned the attention toward naturally abundant eco-friendly dyes, as greener alternatives [14,15], with biodegradability and low toxicity [14]. Examples of natural sources for dyes in DSSCs are spinach, blackberries, raspberries, pomegranates, beetroot, and others with efficiency ranging 0.1 % to 2.0 % [16]. Specifically, natural dyes such as betalains (from red beet, prickly pear) and anthocyanins (from berries, red cabbage) have also shown promise due to their strong visible light absorption and tunable properties [17]. Building upon existing research, studies have shown that flavonoids like Quercitin and Rutin, found in various plants including Juniper [18], were used as visible light sensitizers in DSSCs and yielded efficiencies of 2.15 and 0.71 % respectively [19]. To that end, experimental assessment and prototyping of DSSC devices, based on crude dyes from various plants, were earlier performed as exploratory studies on natural sensitizers. Even when the isolation and purification of dyes yielded better results in terms of photoelectrical performance in some cases they helped in the overall selection of plants as natural dye resources [8,20]. Extracts from natural plants can thus be used as useful sensitizers in DSSCs, by virtue of their ability to absorb visible light photons. As such, the dye molecules are excited, where

* Corresponding authors.
E-mail addresses: a.cheknane@mail.lagh-univ.dz (A. Cheknane), n.selmane@lagh-univ.dz (N. Selmane), hshilal@najah.edu (H.S. Hilal).

https://doi.org/10.1016/j.chemphys.2025.112890
Received 17 April 2025; Received in revised form 20 July 2025; Accepted 7 August 2025
Available online 8 August 2025

electrons go from highest occupied molecular orbitals (HOMOs) to lowest unoccupied molecular orbital (LUMOs). The excited electrons are then injected in the TiO_2 conduction band, move to the external circuit and return to the oxidized redox couple species. On the other hand, the holes move from HOMO to the redox couple, and are then quenched by the oncoming electrons leaving no net charge in the redox couple. This summarizes how dye sensitization occurs in DSSCs.

On paper, such a formalism looks easy and straightforward. However, in practice, things are more difficult. It is known that oncoming solar radiations, that reach earth surface, involve small proportions of UV radiations [21]. Such UV radiations can excite the wide band gap TiO_2 particles themselves, yielding highly oxidizing holes in the valence band. Such holes are capable of oxidizing the dye molecules in the DSSCs, and bleach the redox couples, with time [22]. Instability is thus a serious challenge in DSSCs and needs to be overcome. One way out is adding UV protectors (filters) that are stable molecules with ability to absorb in the UV region [23]. Therefore, visible sensitization and UV protection are two different processes that are both needed in DSSCs.

However, a research gap is identified in screening the large variety of phytochemicals from such botanicals via a deeper investigation in terms of UV protection and cell stability. Exploratory studies on natural dyes could help increase the research speed for improved stability by providing shortcuts toward suitable candidates. Focusing on the fact that natural sensitizers face challenges in stability, more work is thus needed [24]. One effective method is the incorporation of UV absorbers from natural plants, to protect the sensitizers and the redox couples from degradation caused by UV radiation [25].

Herein, we present a preliminary experimental and theoretical evaluation of a number of under-explored botanicals. The goal is to investigate ability of extracts from these botanicals to behave as both visible sensitizers and UV protectors. The results will be useful for future studies in in the areas of manufacturing and assessing new types of DSSCs.

Artemisia campestris, *Rosmarinus officinalis*, Haloxylon scoparium and *Juniperus phoenicea*, all from North African regions, were not described as visible sensitizers and UV protectors for DSSCs, and will be extracted as described in literature [20] and studied here. As such, these botanical plants were not studied in DSSCs to our knowledge [8,11,26,27], vide infra.

The strategy is two-fold, involving both experimental and theoretical parts. In the experimental study, the plants active ingredients are extracted by the Soxhlet method. The extracts are then examined for their potential values as visible sensitizers and UV protectors for natural dye sensitized solar cells (NDSSCs). This will be achieved by studying the electronic absorption properties to determine regions of absorptions. Fourier Transform infrared (FTIR) spectral analysis will be used to check for -OH and -COOH binding functional groups along with aromatic rings that improve electron transfer in DSSCs [28]. TGA results will be used to assess extract thermal stability. The DTA is used to check phase changes that are necessary for DSSCs [29,30].

Theoretical investigation will be conducted on earlier literature phytochemicals, **esculetin-6-O-glucoside** (from *Artemisia Campestris*) [31], **scutellarein** (from *Rosmarinus officinalis*) [32], **3-(2-*N*-acetyl-*N*-methylaminoethyl)indole** (from Haloxylon scoparium) [33] and **3-p-coumaroylquinic acid** (from *Juniperus Phoenicea*) [34]. *Artemisia campestris* is known for its rich phytochemical profile, including flavonoids, coumarins and essential oils [31,35]. Literature described various Artemisia-derived compounds for their antioxidant and antimicrobial properties [36,37]. **Esculetin-6-O-glucoside**, a coumarin glycoside from *Artemisia campestris*, was not harvested for DSSC applications before. *Rosmarinus officinalis*, commonly known as rosemary, has high content of phenolic compounds, particularly flavonoids and diterpenes [32,38]. Compounds like carnosic acid and rosmarinic acid were studied for their antioxidant and photo protective properties [32,38]. Rosemary leaves were harvested to create carbon dots for DSSCs and achieved efficiencies of 6.79–7.32 % [11]. **Scutellarein**, a flavonoid from *Rosmarinus officinalis*, was not previously explored for DSSCs. Haloxylon scoparium is adapted to arid environments and known for its alkaloid content. Previous research was focused on the medicinal properties of Haloxylon-derived compounds, including their antiviral and anticancer activities [33]. Their application in DSSCs remains unexplored, and the **3-(2-N-Acetyl-*N*-methylaminoethyl)indol** is being theoretically considered here as a novel sensitizer for DSSCs. The fourth candidate, *Juniperus communis*, is rich with phenolic acids, flavonoids and essential oils [34], and literature described its antimicrobial and anti-inflammatory properties. In DSSCs, juniper-derived compounds, including **3-p-Coumaroylquinic acid**, were not extensively studied for DSSCs.

These compounds are investigated here by Density Functional Theory (DFT) [39], and Time-Dependent DFT (TDDFT) [40] calculations, using the range-separated functional CAM-B3LYP [41] level of theory. The method is well known for handling long-range interactions, such as charge transfer [42]. It also provides a more balanced treatment of ground-state properties, all as available in the Gaussian 09 W software package [43,44]. Key electronic parameters, such as the electrophilicity index (ω) and the balance of donating/accepting powers (ω^+/ω^-), which highlight stability traits of the selected compounds, are studied. The same computational procedure is applied on the reference dyes Quercitin and Rutin [19] for comparison purposes. Quercetin and Rutin are included solely as computational reference dyes to benchmark the optoelectronic performance of the selected natural phytochemicals. These widely studied flavonoid dyes serve as theoretical baselines and were not experimentally evaluated in this study.

To provide deeper insights into the electronic interactions governing charge transfer efficiency and stability, Natural Bond Orbital (NBO) [45,46] perturbation theory analysis was employed for the first time in this context. The results will assess donor-acceptor interactions in Juniper (3-p-Coumaroylquinic acid) and Rosemary (Scutellarein), supporting efficient charge delocalization and reduced recombination losses. The NBO findings will align with previous electronic structure analyses, including HOMO-LUMO and TDDFT spectra, reinforcing the dye suitability for DSSC applications. Comparing the stabilization energies of these phytochemicals, with those of Quercetin and Rutin, will show if Juniper and Rosemary-derived dyes exhibit superior charge transfer capabilities, making them promising candidates for high-stability UV-protected DSSCs.

Although crude extracts will be experimentally studied, the theoretical calculations in this work focus on key phytochemical constituents identified in the literature for each plant. While the present study aims at investigating the potential of crude extracts themselves for DSSCs, it is not possible to do that theoretically on crude extracts. The extracts involve various additional compounds that influence one another making the calculations not easy. Therefore, the theoretical study is restricted to the dye molecules, described above, commonly abundant in the plants.

To our knowledge, the crude dye extract screening, and the selected natural phytochemicals evaluation, were not previously reported in sensitization and UV protection. The results will open the door to assess more natural botanicals.

2. Experimental

2.1. Materials

Methanol solvent has been delivered by EURL SIALCHIM Company, Tlemcen, Algeria, from HONEYWELL. Methanol is chosen for its effectiveness and superior performance in isolating the types of natural dyes relevant for DSSC applications, such as anthocyanins, betalains, chlorophyll, and carotenoids [8,47]. All other common materials have been purchased form the local market in pure forms.

The studied North African botanical plants Haloxylon scoparium (A), *Rosmarinus officinalis* (B), *Artemisia campestris* (C) and *Juniperus*

phoenicea (D) are presented in Fig. 1. These studied botanicals are selected from North African regions, and have been specifically collected from the Laghouat region in Algeria in 2021. Only the leaves are considered here.

Fig. 2 describes the molecular structures of the investigated natural dyes Esculetin-6-O-glucoside, Scutellarein, 3-(2-N-Acetyl-*N*-methyl-aminoethyl)indole and 3-p-Coumaroylquinic acid, found in *Artemisia Campestris*, *Rosmarinus officinalis*, Haloxylon scoparium and *Juniperus Phoenicea*, respectively, based on literature [32–34]. Esculetin-6-O-glucoside from Artemisia belongs to the coumarin family, well-known for robust photophysical properties [48,49]. This dye involves a coumarin core with a glycosyl moiety at the sixth position indicating high solubility in polar solvents and good interactions with the TiO_2 surface via the free hydroxyl groups [50]. The dye exhibits absorption maxima in the UV range, making it suitable for UV co-sensitization in DSSCs here [51]. Scutellarein from Rosemary, on the other hand, involves flavonoids that are known for their strong light absorption in the visible region [14]. The 3-(2-N-Acetyl-*N*-methylaminoethyl)indol from Haloxylon, presents aindole core that is known for its electron-donating characteristics. Finally, 3-p-Coumaroylquinic acid, extracted from Juniper, incorporates both quinic acid and p-coumaric acid moieties with a carboxylic acid group promising better anchoring capabilities.

2.2. Equipment

A FAITHFUL heating mantle, analytical thimbles, and filtering papers made by PRAT DUMAS France for qualitative analysis, are used in the Soxhlet and maceration setups. A 250 mL Soxhlet apparatus, equipped with a 500 mL round-bottomed flask has been used to obtain concentrated crude dye extracts from studied botanicals [52]. The equipment have been delivered by EURL SIALCHIM Company in Tlemcen. The extraction process has been performed in the Laboratory of Materials, Energy Systems, Renewable Energies and Energy Management (LMSEERGE), Faculty of Technology, Laghouat, Algeria.

The electronic absorption characteristics of the crude dye extracts, dissolved in methanol, are analyzed in the range of 190 to 800 nm on a SHIMADZU UV-1900 UV–Vis spectrophotometer, with a baseline correction using the blank methanol solvent. Functional groups have been analyzed by solid-state FT-IR spectroscopy, on an Agilent Cary-600-FTIR Spectrometer, in the range 350 to 7800 cm^{-1}. FT-IR spectra have been measured at the "Laboratory of Physical Chemistry of Materials (LPCM), Faculty of Sciences (UATL), Laghouat, Algeria". The Thermogravimetric-Differential Thermal analyses (TG-DTA) of solid-state samples are obtained using the LABSYS EVO TG-DTA/DSC available at "Plateau Technique d'Analyses Physico-Chimiques (PTAPC-CRAPC)-LAGHOUAT-Algeria". Measurements have been made under inert gas of N_2(g) flowing at 40 ml/min, with a scan rate of 0.03 °C/min starting from ambient temperature to 600 °C.

2.3. Dye extract preparations

The leaves obtained from the botanical plants have been cleaned using distilled water in a basket and dried from moisture under sunlight for 4 h inside aluminum plates, as described earlier [8,24,29,53]. The dried leaves have then been gently fine-ground in a mortar to ensure concentrated crude dye extracts [54]. A sample (30 g) of each plant fine powder has been placed into the filtering thimble and extracted by the Soxhlet method for around 5 h in ethyl acetate (500 mL). All extracts have then been filtered to ensure the purity and clarity, and stored in the dark [24]. After filtering, the extract solutions have been dried, and resulting dry powders have been analyzed by FT-IR and TG-DTA.

Another portion (15 g) of each plant fine powder has been processed through a quick extraction using the maceration technique in methanol solvent (100 mL). Each mixture has first been quickly agitated at 80 °C for 5 min, then at 40 °C for 2 h. Using a pipet, an extract solution aliquot has been taken from each botanical, filtered and divided into two samples. One sample is used as is (concentrate) and another is diluted for the electronic absorption spectral analysis. The concentrated extract solution has been progressively diluted with methanol until an almost transparent solution is obtained that yields a suitable electronic absorption spectrum with absorbance values within the optimal detection range of the spectrophotometer.

3. Theory

Throughout the years, a theoretical backbone for Dye-Sensitized Solar Cells (DSSC) built upon Density Functional Theory (DFT) and Time Dependent DFT (TDDFT), was under development. It helped in describing and evaluating the properties that governed the DSSC performance and efficiency, including light harvesting efficiency (*LHE*), diffusion constant (*Diff*), ionization potential (*IP*), electron affinity (*EA*) and others [55–59].

3.1. DFT and TDDFT calculations

The theoretical calculations here are conducted on selected isolated phytochemicals representing the main constituents of the plant extracts. These molecules were chosen based on prior phytochemical studies and are hypothesized to contribute significantly to the experimental absorbance features.

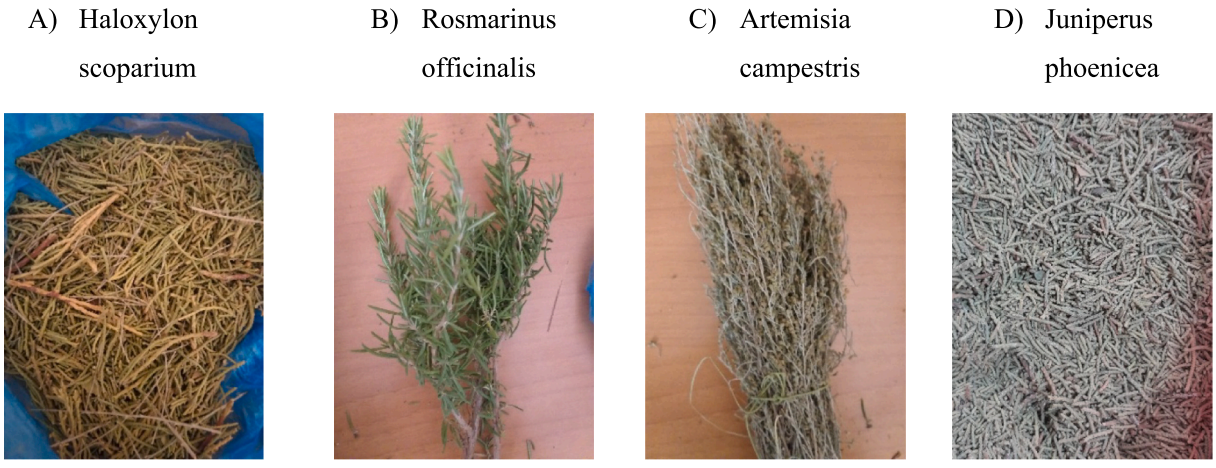

Fig. 1. Photographs of the botanical species investigated in this study. The plants are collected from the Laghouat region (Algerian Saharan Atlas). From left to right: *Artemisia campestris*, *Rosmarinus officinalis*, Haloxylon scoparium, and *Juniperus phoenicea*.

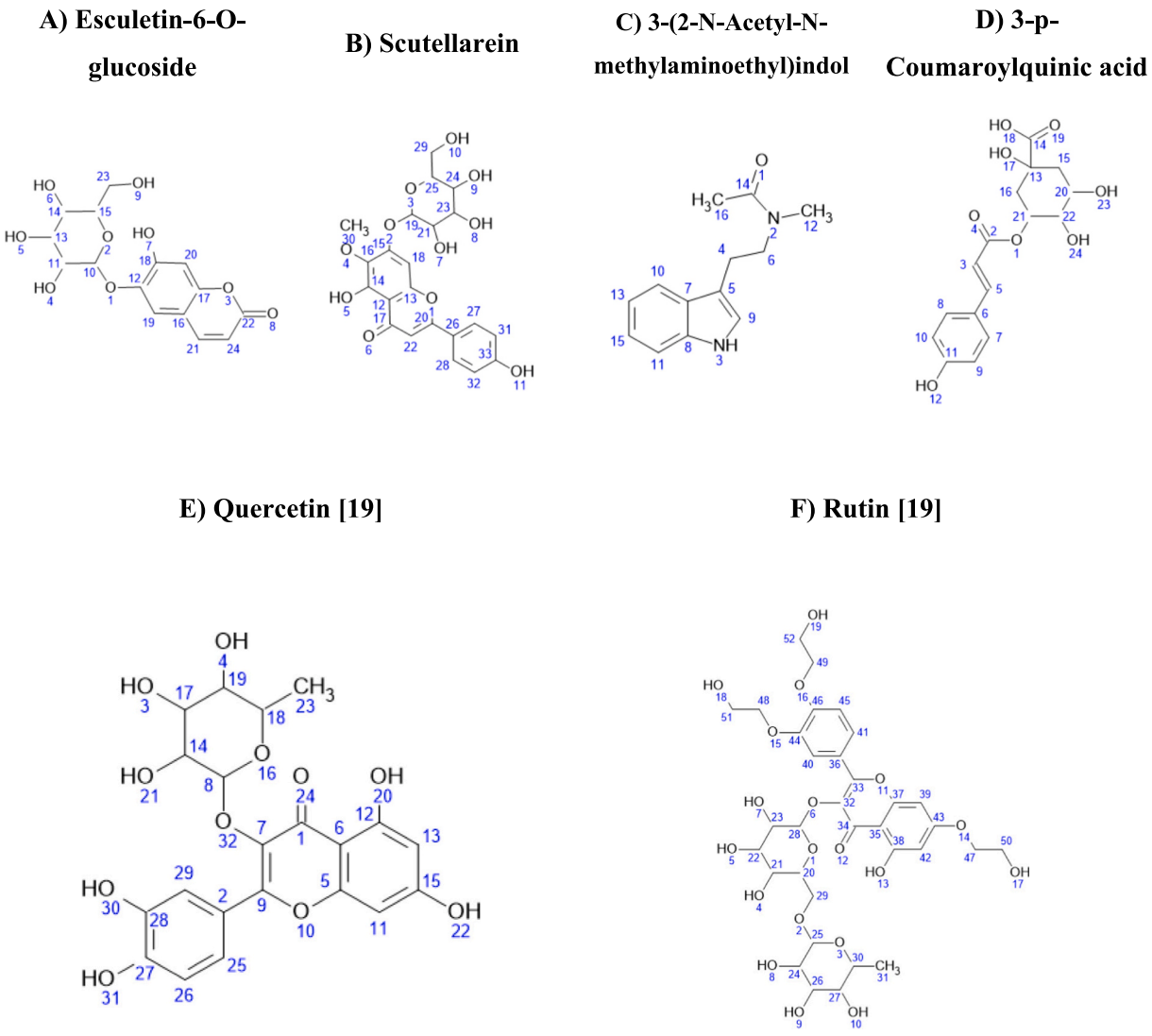

Fig. 2. Chemical structures of selected phytochemicals reported in the literature and associated with the studied plants. (A) *Artemisia campestris*, (B) *Rosmarinus officinalis*, (C) Haloxylon scoparium, and (D) *Juniperus phoenicea.* For benchmarking, reference dyes included are (E) Quercetin and (F) Rutin.

The Density Functional Theory (DFT) and Time-Dependent DFT theory (TD-DFT), have been used here with the Gaussian 09 W software package. The CAM-B3LYP functional has been selected for its proven ability to handle long-range charge-transfer excitations typical of donor-acceptor dye systems. This range-separated hybrid functional mitigates self-interaction errors and has shown reliable performance in modeling photoexcited states of organic DSSC dyes in prior studies [60,61]. The 6-311G(d,p) basis set is chosen as it provides a good balance between computational cost and accuracy for organic molecules with π-conjugated systems. Solvent effects have been incorporated via the conductor-like polarizable continuum model (CPCM) with methanol as the solvent, to mirror the experimental environment during extraction and spectroscopy. All optimized structures have been confirmed to be at local minima by the absence of imaginary frequencies. The TD-DFT calculations have been performed to evaluate the excited-state properties, calculating up to 12 excited states per compound (using nstates = 12). Post-processing analysis of the molecular orbitals has been conducted, focusing on the HOMO-LUMO gaps, and on the nature of the electronic transitions, to assess the potential for electron injection into the conduction band of TiO_2, along with other properties. The oscillator strengths are also extracted from the TD-DFT results to estimate the *LHE* of each compound. Additionally, qualitative benchmarking of the theoretical electronic absorption spectra with experimental measurements was performed. The observed absorption maxima and oscillator strengths of key phytochemicals (e.g., Scutellarein, 3-p-Coumaroylquinic acid) are in reasonable agreement with experimental spectra of the crude extracts, supporting the validity of the computational approach.

3.2. Photovoltaic performance parameters

3.2.1. Light-harvesting efficiency (LHE)

LHE is important for estimating the ability of sensitizers to convert photons into electrical energy. At maximum absorption, *LHE* can be calculated using Eq. (1), where higher values indicate improved absorption and, consequently, more electronic injection and higher DSSC performance [58,62,63]:

$$\mathrm{LHE} = 1 - 10^{-f} \tag{1}$$

where f is the oscillator strength of wavelength at maximum absorption, obtained from TD-DFT calculations.

3.2.2. Diffusion constant (Diff)

Diff describes the rate at which dye molecules diffuse within the DSSC electrolyte. The Stokes-Einstein relation, Eq. (2), is used to compute the dye-molecule diffusion constants [64,65]:

$$\mathrm{Diff} = \frac{\mathrm{kT}}{6\pi \mathrm{n}_0 \mathrm{r}_{\mathrm{dye}}} \tag{2}$$

where k is Boltzmann's constant, T is the kelvin temperature, n_o is the medium viscosity (approximated to that of helium at 300 K), and r_{Dye} is the dye molecular radius.

A higher diffusion constant decreases aggregation and improves uniform dye distribution on the TiO_2 surface, promoting better electron injection [65].

3.2.3. Dye molecular radius (rDye)

The r_{Dye} value determines how well the dye molecules adhere to the TiO_2 surface, and interact with the electrolyte. It is calculated by Eq. (3) [28].

$$\mathrm{r}_{\mathrm{Dye}} = \sqrt[3]{\frac{3\mathrm{M}}{4\pi\rho \mathrm{N}_{\mathrm{A}}}} \tag{3}$$

where M is the dye molar mass, ρ is the density of the solvent, and N_a is Avogadro's number.

3.2.4. Frontier molecular orbital analysis (HOMO/LUMO)

The theorem of Koopmans suggests that examining the Frontier Molecular Orbital energies of a molecule helps understand its overall characteristics. Hence, the HOMO and the LUMO reflect possibilities of the molecule to participate in electrophilic or nucleophilic reactions [57,66,67]. In addition, for improved DSSC performance, the dye *LUMO* should be at a higher (less negative) potential than the conduction band edge of TiO_2 (−4.0 *eV*). This alignment ensures efficient and rapid electron injection from the excited dye (*LUMO*) to the TiO_2 conduction band. On the other hand, the dye HOMO should be at a lower (more negative) potential than the I^-/I_3^- redox potential (−4.8 *eV*) to ensure effective dye regeneration [68]. The energy gaps between the excited dye (*LUMO*) and the TiO_2 conduction band edge (ΔE_{LC}), and between the dye *HOMO* and the I^-/I_3^- redox couple potential (ΔE_{RH}), are detailed in Eqs. (4) and (5):

$$\Delta \mathrm{E}_{\mathrm{LC}} = \mathrm{E}_{\mathrm{LUMO}} - \mathrm{E}_{\mathrm{CB}} \tag{4}$$

$$\Delta \mathrm{E}_{\mathrm{RH}} = \mathrm{E}_{\mathrm{redox}} - \mathrm{E}_{\mathrm{HOMO}} \tag{5}$$

3.2.5. Ionization potential (IP) and electron affinity (EA)

IP and *EA* are defined by the Eqs. (6) and (7), respectively. *IP* represents the minimum energy required to remove an electron from a neutral atom (or a molecule) in its ground state corresponding to the negative value of the *HOMO* energy level. Lower *IP* values indicate more efficient dye regeneration. *EA* represents the energy change when an electron is added to a neutral atom (or molecule), calculated as the negative value of the *LUMO* energy level. Higher *EA* means more efficient electron injection [64,69]:

$$\mathrm{IP} = -\mathrm{E}_{\mathrm{HOMO}} \tag{6}$$

$$\mathrm{EA} = -\mathrm{E}_{\mathrm{LUMO}} \tag{7}$$

3.2.6. Electronic chemical potential (μ) and chemical hardness (η)

The electronic chemical potential (μ) described by Eq. (8) is a thermodynamic indication on how easily an electron can be added to a system. In DSSCs, a lower electronic chemical potential is desirable because it implies enhanced electron transfer due to easier electron acceptance [70].

The chemical hardness (η) defined by Eq. (9) describes the stability of the molecule against electron transfer. Higher η indicates higher molecule resistance to changes in its electronic configuration, thus higher stability. However, in DSSCs a balance off is needed. While stability is important, excessive chemical hardness would limit the necessary electron transfer processes. Therefore, to optimize charge transfer and separation efficiency, the dye should not possess too high η [69].

$$-\mu = \frac{1}{2}(IP + EA) = \chi \tag{8}$$

$$\eta = \frac{1}{2}(\mathrm{IP} - \mathrm{EA}) \tag{9}$$

where χ represents the electronegativity, defined here as ability of a molecule to accept an electron.

3.2.7. Electrophilicity index (ω) and donating/accepting powers (ω^+/ω^-)

The electrophilicity index (ω), defined in Eq. (10) is a measure of the molecular ability to accept additional negative charges from its environment. A higher electrophilicity index is preferred in DSSCs as it indicates better electron transfer [71]. This measure is evaluated based on two factors: the electrophilic propensity to acquire an additional negative charge represented by μ^2, and the system resistance to negative charge exchange characterized by chemical hardness (η). These concepts are summarized in Eqs. (9) and (10):

$$\omega = \frac{\mu^2}{\eta} \tag{10}$$

Electron-accepting and electron-donating powers control the molecule ability to partially accept or donate a negative charge, with preferably higher values of the latter [59,62,72,73]. Electron donating power (ω^+) and electron accepting power (ω^-) are represented by Eqs. (11) and (12). A higher electron accepting power means the molecule accepts electrons easier, which limits recombination factors and charge losses. A higher electron donating power is also beneficial, as it facilitates electron transfer [74].

$$\omega^- \approx \frac{(\mathrm{IP} + 3\mathrm{EA})^2}{16(\mathrm{IP} - \mathrm{EA})} \tag{11}$$

$$\omega^+ \approx \frac{(3\mathrm{IP} + \mathrm{EA})^2}{16(\mathrm{IP} - \mathrm{EA})} \tag{12}$$

According to Parr and Yang's formulations, the values of μ, η and ω are interrelated as shown in Eqs. (8–10) [75,76].

3.2.8. Natural bond orbital (NBO) analysis

Natural Bond Orbital (NBO) analysis provides insights into the electronic interactions within a molecule by describing electron delocalization, donor-acceptor interactions and stabilization effects. This method is particularly useful in evaluating charge transfer efficiency, which plays a crucial role in the DSSC organic dye performance. Through second-order perturbation theory, the strength of these interactions can be assessed, allowing for a better understanding of charge mobility and electronic stability [45,46,58]. The electronic properties of the studied dyes have been discussed above through DFT and TDDFT analyses, where HOMO-LUMO gaps, density of states (DOS) and electronic absorption spectra are examined. These studies provide an initial understanding of charge transfer properties. Moreover, NBO analysis adds another layer of depth by explicitly quantifying orbital interactions and electron delocalization within the molecular framework. By correlating NBO results with theoretical findings from electronic structure analysis and experimental electronic absorption spectra, the suitability of the studied dyes for DSSC applications can be predicted.

In this study, NBO calculations are performed using the NBO 3.1 module in Gaussian 09 W with the same computational setup as the DFT calculations: CAM-B3LYP/6-311G(d,p) in methanol (CPCM solvation model). The key focus is on second-order perturbation theory analysis, which quantifies donor-acceptor interactions in terms of energetic stabilization. The analysis aims at determining the strength of charge delocalization and identifying key orbital interactions relevant to electron transfer. By examining stabilization energy $E(2)$ values, it is

possible to identify strong π-π* conjugation and lone-pair interactions, which are critical in facilitating efficient charge transfer. Molecules exhibiting higher $E(2)$ stabilization energies typically have better charge delocalization [77,78], lower electron recombination rates and improved electron injection into the semiconductor [79]. Dyes with strong donor-acceptor orbital interactions with significant stabilization energy values are expected to exhibit enhanced photovoltaic properties in DSSCs [78], as they can facilitate efficient electron movement from the dye to the TiO_2 conduction band. To ensure consistency and reliability, the results are processed using an automated Python script developed to extract and filter NBO parameters from Gaussian output files. The script applies filtering criteria to select only significant interactions based on stabilization energy cutoffs, allowing for a more focused and meaningful interpretation of the data. This ensures that only the most relevant donor-acceptor interactions are considered in the final analysis. The discussion of these results is expanded in subsection 4.2.c, where detailed donor-acceptor interactions, energy transfer pathways and their implications in DSSC applications are analyzed. Tables 4–9 present the extracted second-order perturbation interactions, providing a comparative view of the stabilization energies across different dye molecules. By combining NBO perturbation theory with previously discussed electronic absorption spectral properties and electronic structure analysis, a convincing justification of the dyes, as promising DSSC candidates, is thus provided.

4. Results and discussion

4.1. Experimental results

4.1.1. Electronic absorption spectra

Electronic absorption spectra measured for the crude dye methanolic extracts from *Artemisia campestris*, Haloxylon scoparium, *Juniperus phoenicea* and *Rosmarinus officinalis*, in 190 to 800 nm range, are depicted in **Figs. 3(a)** and **(b)**. As stated above, the experimental spectra are for the crude extract, while the TDDFT simulations are for individual phytochemicals. The observed spectral features likely result from a synergistic overlap of multiple dye molecules, including the ones modeled here.

The spectra for various concentrated extracts, Fig. 3(a), demonstrate peaks within the visible spectrum with notable similarity between the absorption profiles for the four investigated botanicals. Two strong absorption bands are observed, one in the range 400–500 nm, and another spanning the range 650–700 nm.

Based on the absorption analysis yields, the crude extracts possibly contain chlorophylls, flavonoids, anthocyanins, carotenoids and coumarins, as confirmed by the blueprints of each pigment. For instance, chlorophyll absorbs at around 430, 660 and 670 nm [14]. Anthocyanin and flavonoids contribute to the absorption, with anthocyanins affirmed by absorbing between 450 and 700 nm [14,27] and flavonoids between 350 and 500 nm [14]. Zooming further, small bumps are observed in the spectra, one at 540 nm indicating possible presence of betalains and carotenoids [80,81], and one at 600 nm possibly related to chlorophyll *b* [82,83].

Fig. 3(b) depicts results for the diluted extract solutions to have a closer look at the crude dye extract behavior in the UV range. Relatively strong UV absorptions, with peaks in the 200–400 nm range, confirm UV activity.

The results demonstrate the capacity of the extract constituents to capture radiations through a wide range, spanning both UV and reaching the near IR regions. This is a useful feature for application in DSSCs [12]. The results thus confirm the extracts usefulness in both sensitization and UV protection. This highlights the potential importance of the extracts in NDSSCs.

4.1.2. FTIR spectra

Solid state FTIR spectra are depicted in Fig. 4, for samples dried from plant extracts under investigation, *Artemisia campestris* (ART), Haloxylon scoparium (HLX), *Juniperus Phoenicea* (JNP), and *Rosmarinus officinalis* (RSM). The Figure shows the similar vibrational modes. The bands at ~3400 cm^{-1} are due to O—H stretching vibrations, probably for phenolic compounds. Other intense sharp bands appear in all extracts at ~1600 cm^{-1}, due to C═C stretching vibration indicating the aromatic nature of the dye components. Peaks in the range 1200–1700 cm^{-1} also confirm the various hydroxyls, carbonyls and other functional groups characteristic of phenolic and flavonoid compounds. These functional groups provide the dual role of light absorption and electron transfer. The functional groups are necessary to chemically bind dye molecules with the TiO_2 surface OH groups in the DSSCs and to improve electronic injection [84].

4.1.3. Thermogravimetric analysis (TGA)

TGAs of solid samples dried from crude dye extracts of Haloxylon (HLX), Artemisia (ART), Juniper (JNP), and Rosemary (RSM), are presented in Fig. 5. The Figure shows a two-step mass loss process in all

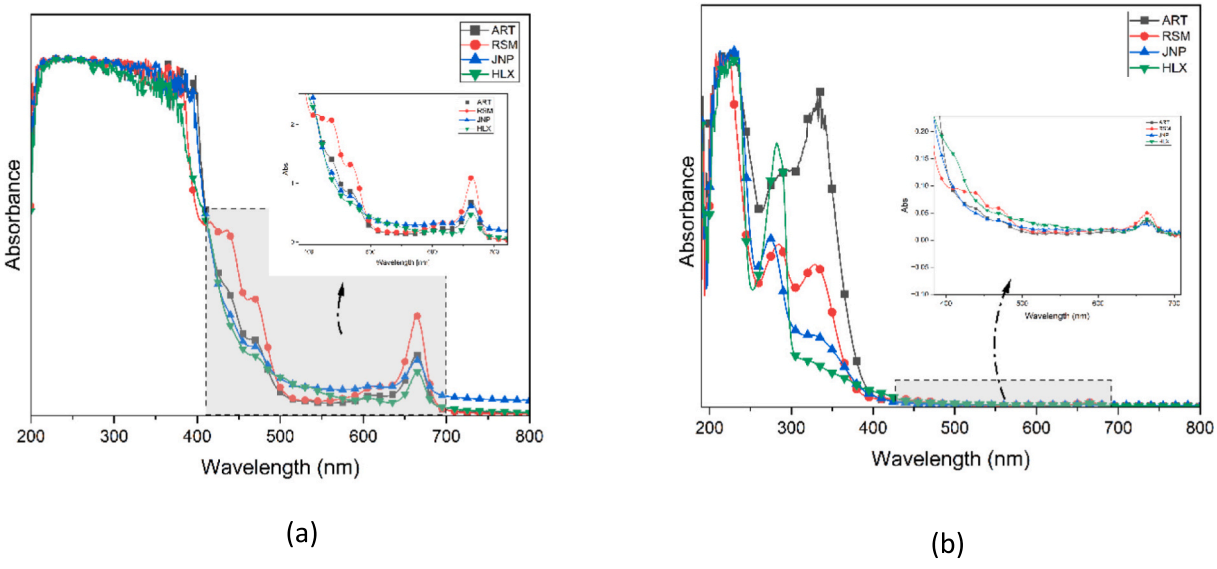

Fig. 3. Electronic absorption spectra of crude extracts from various extracts in methanol. (a) concentrated extracts and (b) diluted extracts. Spectra are shown for extracts from *Artemisia campestris* (ART), Haloxylon scoparium (HLX), *Juniperus phoenicea* (JNP), and *Rosmarinus officinalis* (RSM).

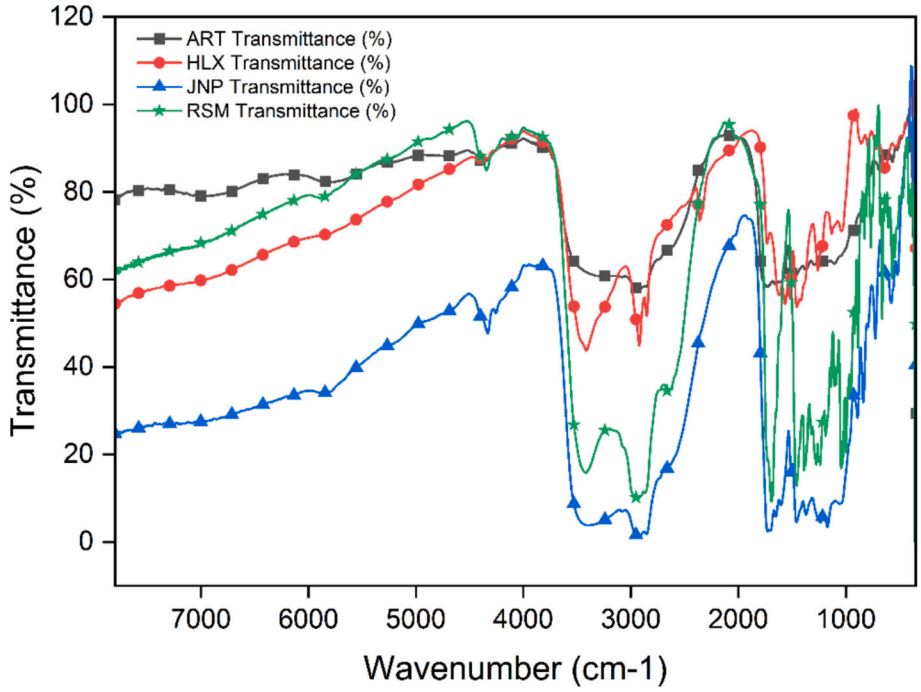

Fig. 4. FTIR spectra measured for solid-state residues obtained from various crude extracts. The extracts are taken from Haloxylon scoparium (HLX), *Artemisia campestris* (ART), *Juniperus phoenicea* (JNP), and *Rosmarinus officinalis* (RSM).

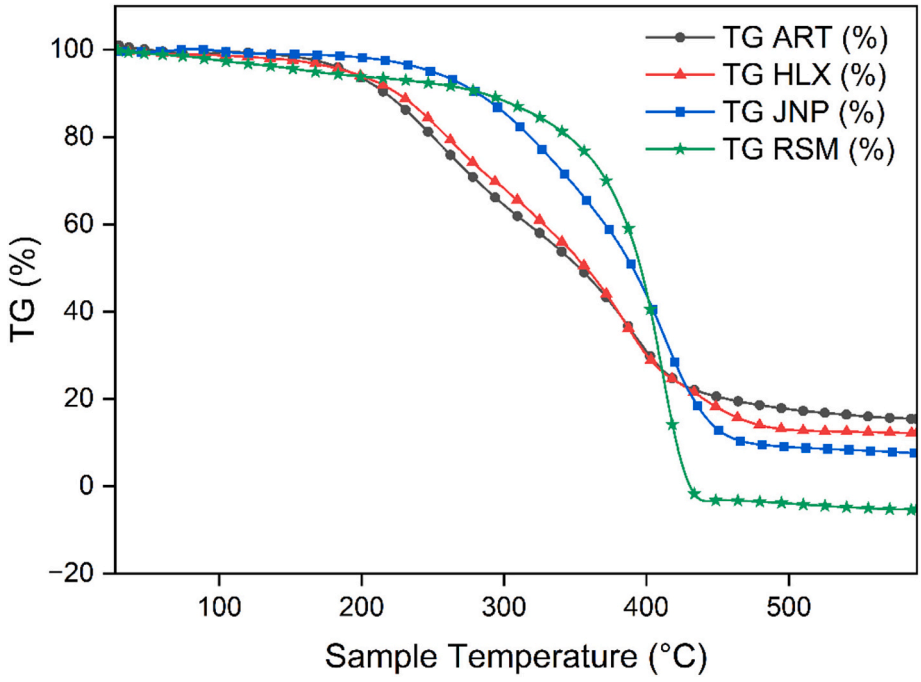

Fig. 5. TGA curves measured for solid residues derived from various crude extracts. The extracts are taken from Haloxylon scoparium (HLX), *Artemisia campestris* (ART), *Juniperus phoenicea* (JNP), and *Rosmarinus officinalis* (RSM).

botanicals with similar behaviors. For instance, the first significant weight loss at ~100 °C, is attributed to the evaporation of volatile organic compounds and moisture from the solids. With increased temperature, a notable decomposition phase begins at ~250 °C and continues to ~400 °C. This describes the breakdown of the complex organic molecules, possibly phenolic constituents, which tend to be relatively thermally stable. The residual masses beyond 450 °C indicate that the extracts contain compounds that remain thermally stable even at higher temperatures. The TGA results thus confirm thermal stability, which is crucial for long-term performance under temperature.

4.1.4. *Differential thermal analysis (DTA)*

DTA results, Fig. 6, provide comparative thermal profiles for the four solids obtained from the extracts of Haloxylon scoparium (HLX), *Artemisia campestris* (ART), Juniper phoenicea (JNP) and Rosemary officinalis (RSM). Haloxylon presents a clear endothermic behavior in the

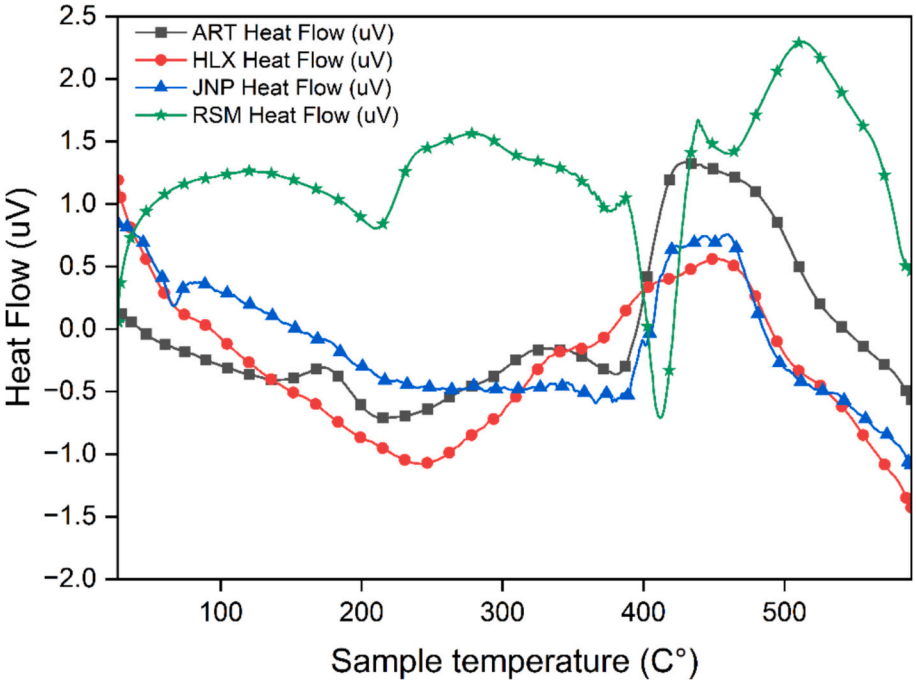

Fig. 6. DTA curves measured for solid residues obtained from crude extracts. The extracts are taken from Haloxylon scoparium (HLX), *Artemisia campestris* (ART), *Juniperus phoenicea* (JNP), and *Rosmarinus officinalis* (RSM).

a

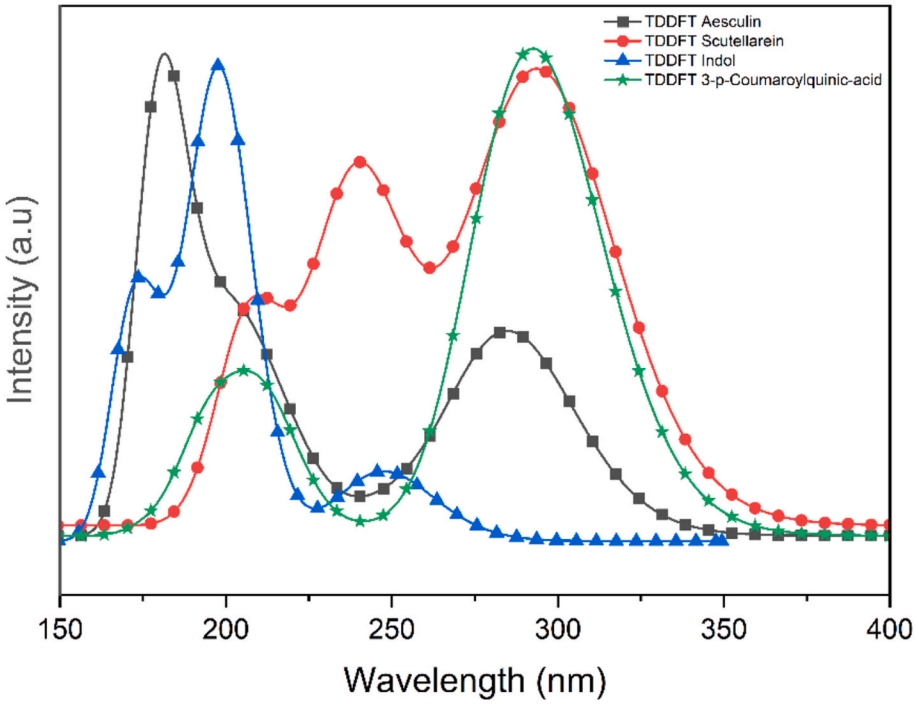

Fig. 7. TDDFT-simulated absorption spectra for the investigated dyes using the CAM-B3LYP/6-311G(d,p) level of theory in methanol. (a) Combined theoretical spectra for Esculetin-6-O-glucoside, Scutellarein, 3-(2-N-Acetyl-*N*-methylaminoethyl)indol, and 3-p-Coumaroylquinic acid. (b-e) Comparison between theoretical spectra (in methanol) and corresponding experimental electronic absorption spectra of the crude extracts from *Artemisia campestris*, *Rosmarinus officinalis*, Haloxylon scoparium and *Juniperus phoenicea*, respectively.

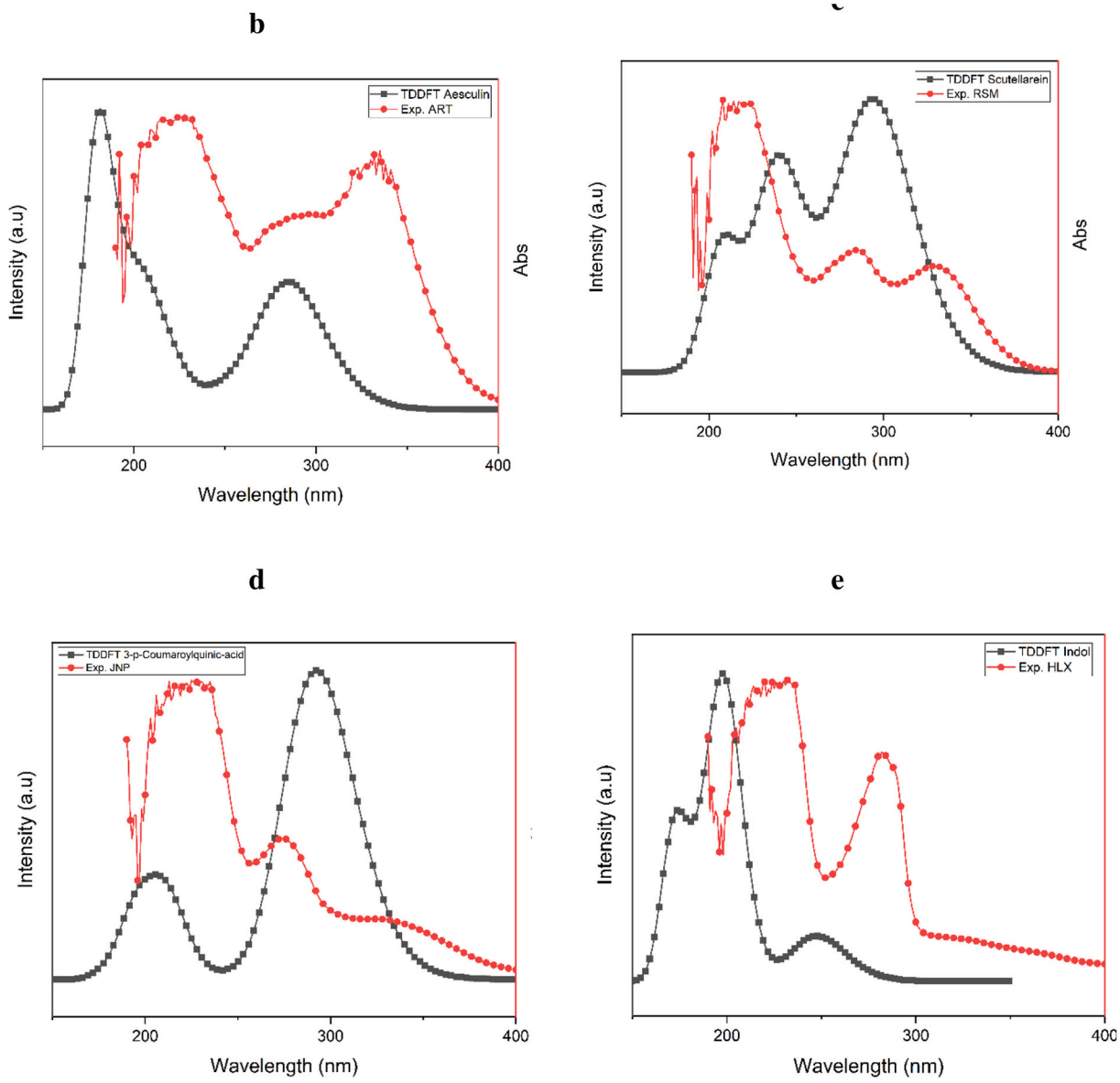

Fig. 7. (*continued*).

range 200–300 °C, describing the evaporation of residual moisture or solvent, then, an exothermic behavior is detected at above 400 °C indicating oxidation and combustion due to organic decomposition. Artemisia exhibits wide endothermic peaks in the range 100 to 400 °C. At above 400 °C a more significant exothermic process appears, compared to Haloxylon, appears. Juniper behavior resembles Haloxylon with a wider endothermic peak. The immense energy release with thermal oxidation in Artemisia indicates a high organic content that combusts efficiently. On the other hand, Rosemary shows a more complicated thermal behavior with several exothermic peaks distributed over the whole temperature range with a sharp endothermic peak at ~420 °C. DTA curves for the thermal characteristics of the studied natural components, confirm their thermal stability and suitability for DSSCs.

4.2. Theoretical results

4.2.1. Excited state analysis

The excited state transitions of the dyes Esculetin-6-O-glucoside, Scutellarein, 3-(2-N-Acetyl-*N*-methylaminoethyl)indol and 3-p-

Table 1
DDFT results* for Esculetin-6-O-glucoside, Scutellarein, 3-(2-N-Acetyl-*N*-methylaminoethyl)indol, and 3-p-Coumaroylquinic acid in methanol. The dyes represent key phytochemicals from *Artemisia campestris*, *Rosmarinus officinalis*, Haloxylon scoparium, and *Juniperus phoenicea*, respectively.

Dyes	λ_{max} [nm]	Oscillator strength *f* [arbitrary unit]
	TD-DFT CAM-B3LYP	
Esculetin-6-O-glucoside	285.60	0.42
Scutellarein	298.89	0.64
3-(2-N-acetyl-*N*-methylaminoethyl) indol	250.81	0.10
3-p-Coumaroylquinic acid	292.54	1.02
Quercitin	309.85	0.59
Rutin	312.31	0.73

* TDDFT calculations performed at the CAM-B3LYP/6-311G(d,p) level with solvent effects modeled using CPCM (methanol).

Coumaroylquinic acid, dissolved in methanol, are described in Fig. 7 and summarized in Table 1. The TD-DFT, by CAM-B3LYP functional with the basis set 6-311G (d,p), is used. In Esculetin-6-O-glucoside from Artemisia, a maximum absorption peak is observed at 285.60 nm with an oscillator strength of 0.42, suggesting a weaker absorption than both reference dyes Quercitin and Rutin (f = 0.59, 0.73). The strong absorption in the UV region is depicted in Fig. 7(a). Scutellarein from *Rosmarinus Officinalis*, Fig. 7(a), has a λ_{max} at 298.89 nm being the closest maximum to Quercitin (λ_{max} = 309.85 nm), with a higher oscillator strength of 0.64, as described in Table 1. This highlights its good UV absorption, with peaks at around 240 nm and 300 nm in Fig. 8 (a). On the other hand, 3-(2-N-Acetyl-*N*-methylaminoethyl)indol from Haloxylon scoparium shows absorption at λ_{max} at 250.81 nm with an extremely low oscillator strength of 0.10. 3-p-Coumaroylquinic acid, from *Juniperus phoenicea*, extends its absorption into the near-UV region, with a λ_{max} of 292.54 nm and a highest oscillator strength of f = 1.02, surpassing both Quercitin and Rutin (f = 0.59, 0.73).

The four compounds show good absorptions in the UV portion, covering the wavelengths at 200, 220, 240, 280 and 300 nm, with variably high oscillator strengths compared to reference dyes Quercitin and Rutin. This feature, together with effective UV absorptions, makes these dyes promising candidates to enhance both light-harvesting efficiency and stability in DSSCs.

The experimental electronic absorption spectral results align with the theoretical ones, as illustrated in Figs. 7**(b-e).** Furthermore, small shifts are noticed with close enough consistency in all four spectra (a, b, c and d) strengthening theoretical yields and confirming the presence of the studied phytochemicals.

4.2.2. *Electronic structural analysis*

Properties of natural dyes follow clear patterns that indicate their potential use in UV protection for DSSCs. While the experimental data are based on crude dye extracts, the theoretical findings directly describe the four dyes themselves, Esculetin-6-O-glucoside, Scutellarein, 3-(2-N-Acetyl-*N*-methylaminoethyl)indol and 3-p-Coumaroylquinic acid. It is thus necessary to address how these can complement other sensitizers in DSSCs, especially with regard to improved UV protection.

Basically, Table 2 describes the theoretical results with differences among the electronic properties of the selected four phytochemicals against the reference dyes Quercitin and Rutin [19]. Artemisia, represented by Esculetin-6-O-glucoside, has the lowest HOMO energy at −7.72 eV, which indicates less charge recombination phenomena leading to better charge transfer. Literature [85] also confirmed that lower HOMO levels lead to lower recombination and charge losses, but extremely low HOMO may negatively affect electron donating capability. Its LUMO value of −0.72 eV, supplemented with highest ΔE_{LH} of 7.00 eV, indicates that the molecule has a wide energy gap, which generally correlates with better photo stability but lower visible light absorption. With a moderate oscillator strength (f = 0.42) this dye alone may not exhibit high *LHE*. The dye is thus a suitable UV absorber but not an effective sensitizer. Its Gibbs free energy is −1258.2 Hartree. This means the dye is stable, with *EA* of 0.72 eV lower than those of Quercitin and Rutin (*EA* = 1.30 and 1.07 eV, respectively), and may be used as a UV protector, combined with another visible light sensitizer in a co-sensitization mode. This shows the tendency to avoid absorption overlap, to ensure energy alignment between the used sensitizers for better *LHE* and to decrease undesirable interactions between the dye molecules. The ΔE_{LC} value 3.28 eV places the LUMO well above the TiO_2 conduction band edge (−4.0 eV), which facilitates electronic injection. However, the relatively high gap compared to Quercitin and Rutin (ΔE_{LC} = 2.70 and 2.93 eV, respectively) may lead to lower power conversion efficiency (*PEC*). Note that Rutin with higher gap exhibits low *PEC*, of 0.71 %, compared to that of Quercitin with 2.15 % [19]. However, its close ΔE_{RH} value (2.92 eV) to Quercitin value at 2.87 eV confirms its stability during redox reactions.

Rosemary, with Scutellarein dye, shows a slightly higher HOMO energy at ∼ − 7.64 eV and a LUMO value of −0.95 eV. This leads to an energy gap of ΔE_{LH} = 6.69 eV that is slightly bigger than Quercitin (ΔE_{LH} = 6.38 eV) [19] and Rutin (ΔE_{LH} = 6.31 eV) [19]. This confirms its slightly higher ability to absorb UV light, compared with Artemisia. However, its high oscillator strength (f = 0.64) ensures better light absorption capability than both reference dyes Quercitin and Rutin (f = 0.59 and 0.73, respectively). The Gibbs free energy (−1678.39 *Hartree*) being greater than that of Quercitin (Gibbs = −1639.16) is a better indicator for higher thermodynamic stability. Among the investigated dyes, its highest electron affinity (*EA* = 0.95 eV) that is closer to the reference dyes Quercitin and Rutin (*EA* = 1.30 and 1.07 eV, respectively), also indicates better electron acceptance ability. This is an

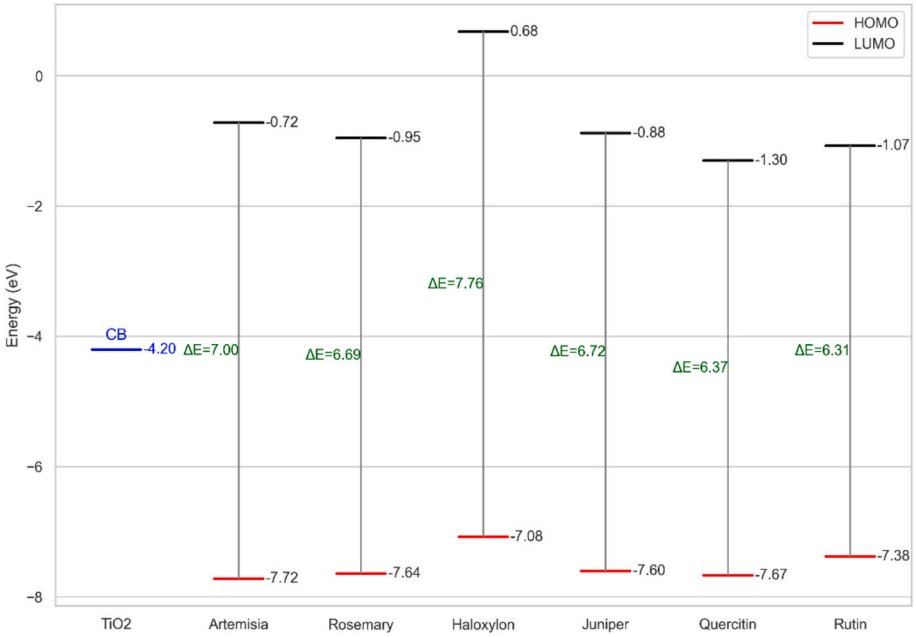

Fig. 8. HOMO-LUMO energy level diagram for various investigated dyes. Calculations are made using the CAM-B3LYP/6-311G(d,p) level of theory in methanol (CPCM).

Table 2
Frontier orbital energy values and related descriptors obtained from CAM-B3LYP/6-311G(d,p) calculations* in methanol (CPCM) for the investigated dyes.

Natural dyes source	HOMO [eV]	LUMO [eV]	*f*	Mass [g/Mol]	Gibbs [eh]	ΔE_{LC} [eV]	ΔE_{RH} [eV]	ΔE_{LH} [eV]	*IP* [eV]	*EA* [eV]
Artemisia	−7.72	−0.72	0.42	340.28	−1258.2	3.28	2.92	7.00	7.72	0.72
Rosemary	−7.64	−0.95	0.64	462.40	−1678.39	3.05	2.84	6.69	7.64	0.95
Haloxylon	−7.08	0.68	0.10	216.28	−689.36	4.68	2.28	7.76	7.08	−0.68
Juniper	−7.60	−0.88	1.02	338.31	−1221.90	3.12	2.80	6.72	7.60	0.88
Quercitin	−7.67	−1.30	0.59	448.38	−1639.16	2.70	2.87	6.38	7.67	1.30
Rutin	−7.38	−1.07	0.73	742.68	−2710.89	2.93	2.58	6.31	7.38	1.07

* All theoretical values are from the present calculations.

important property to stabilize the dye toward photo degradation, making it suitable for co-sensitization. Among the investigated dyes, Scutellarein with lowest ΔE_{LC} of 3.05 eV, that is comparable with Quercitin and Rutin (ΔE_{LC} = 2.70 and 2.93 eV, respectively), exhibits high charge transfer tendency. Scutellarein thus exhibits good compatibility with TiO_2 conduction band edge, in addition to higher compatibility with redox couple (I_3^-/I^-) owing to the ΔE_{RH} value of 2.84 eV. Moreover, it exhibits slightly higher oxidative stability than Esculetin-6-O-glucoside and other candidates.

3-(2-N-Acetyl-*N*-methylaminoethyl)indol from Haloxylon exhibits a HOMO of −7.08 eV, highest LUMO of 0.68 eV and highest ΔE_{LH} of 7.76 eV determining its lower charge injection capabilities. Its lowest oscillator strength, f = 0.10, suggests that this compound would possess lower efficiency as a sensitizer in visible light absorption. With its small ΔE_{RH} of 2.28 eV and low Gibbs free energy of −689.36 Hartree, it may be more prone to instability under redox conditions. Further, its *EA* of −0.68 eV underlines this and indicates that despite its strong UV absorption, careful consideration must be given toward its stability in DSSCs. Furthermore, its extremely high ΔE_{LC} (4.68 eV) suggests high charge losses and charge recombination possibilities.

3-p-Coumaroylquinic acid resembles Rosemary dye. It has HOMO = −7.60 eV and LUMO = −0.88 eV, with ΔE_{LH} = 6.72 eV, slightly higher than that of Scutellarein. This indicates a balance off between stability and absorption. Its oscillator strength (f = 1.02) is also higher than all dyes in this study, indicating a strong light absorption. This is supported by its negative Gibbs free energy of −1221.90 Hratree, which means a stable thermodynamic profile. Its electron affinity is equal to 0.88 eV, suggesting similar redox activity and photostability in action with Scutellarein, rendering this compound a good candidate for protection against UV. Values of ΔE_{LC} = 3.12 eV and ΔE_{RH} = 2.80 eV predict it to be efficient in redox reactions, but not the best electron donor.

Furthermore, Fig. 8 draws attention to the energy alignment of the HOMO and LUMO levels of the investigated dyes relative to the TiO_2 conduction band (CB) at −4.20 eV. Effective DSSC sensitizers must possess a LUMO level higher (less negative) than the TiO_2 CB to ensure efficient electron injection, and a HOMO level low enough to enable regeneration by the redox electrolyte. All dyes satisfy the condition for electron injection, with LUMO energies ranging from −1.30 eV (Quercetin) to +0.68 eV (Haloxylon). However, Haloxylon dye has the largest HOMO-LUMO gap (ΔE = 7.76 eV), which correlates with poor light absorption and low oscillator strength (f = 0.10), as previously discussed. In contrast, Quercetin and Rutin exhibit narrower gaps (ΔE = 6.37 eV and 6.31 eV, respectively), aligning well with their known spectral properties and relatively higher calculated *LHE* values. Among the newly studied dyes, Juniper's 3-p-Coumaroylquinic acid displays a favorable HOMO of −7.60 eV and LUMO of −0.88 eV (ΔE = 6.72 eV), closely matching Rosemary's Scutellarein (ΔE = 6.69 eV). Both show LUMO levels well above the TiO_2 CB, indicating good electron injection capability, while their moderate band gaps and high oscillator strengths suggest strong sensitization potential. Artemisia's dye, with a ΔE of 7.00 eV and a very low LUMO of −0.72 eV, lies closer to the TiO_2 CB limit, possibly reducing injection efficiency. However, its broad UV absorption and stability may support a complementary role as a UV-protective co-sensitizer.

The electrochemical properties are summarized in Table 3, where the dye appropriateness for DSSC applications is readily ascertained. The values of the chemical hardness (η) confirm the trends that Artemisia (−4.22 eV), Juniper (−4.24 eV) and Rosemary (−4.29 eV) are more stable than Haloxylon (−3.20 eV), and are comparable to the reference dyes Quercitin and Rutin (η = −4.48, −4.23 eV, respectively). Haloxylon, while having the lowest hardness, also has the smallest electrophilicity index (ω = 2.63), which may indicate that in some configurations its reactivity can be an asset despite being unstable. On the other hand, the electrophilicity index of Rosemary 5.51 is comparable to that of Rutin 5.66, indicating that Rosemary balances stability and reactivity better than Artemisia at 5.09. The *LHE* values indicate that the potentials of both Rosemary 76.87 % and Juniper 90.45 % are very strong toward effective light absorption, and can provide better light harvesting than the reference dyes Quercitin and Rutin (*LHE* = 74.39 and 81.89 %, respectively). On the other hand, Artemisia exhibits modest *LHE* of 62.05 %, while Haloxylon with the lowest value at 20.57 % could give complementary UV absorption at lower efficiencies. Fig. 9 provides a clearer representation of the *LHE* variation trends across the studied dyes.

For Rosemary's Scutellarein, the diffusion coefficient (*Diff*) 4.02 × 10^{-10} m^2/s resembles that for Quercitin 4.06 × 10^{-10} m^2/s, while the highest value is demonstrated by Haloxylon at 5.18 × 10^{-10} m^2/s. This indicates that the performance may not be exclusively controlled by the diffusion process during the design of DSSCs based on such dyes.

Further analysis of the electrochemical properties, presented in Table 3, gives more information on reactivity and stability for the four dyes. Electronegativity χ is a key parameter characterizing the ability of a molecule to attract electrons. Rosemary, with Scutellarein, presents the highest electronegativity value (χ = 4.29 eV) among the investigated

Table 3
Electrochemical descriptors* of the investigated dyes calculated at the CAM-B3LYP/6-311G(d,p) level in methanol (CPCM).

Dye	η [eV]	μ [eV]	χ [eV]	ω [ratio]	ω- [ratio]	ω+ [ratio]	*LHE* [%]	*Diff* [m^2/s]	*rDye* [m]
Artemisia	−4.22	3.50	4.22	5.09	0.87	5.09	62.05	4.46 × 10^{-10}	2.47 × 10^{-8}
Rosemary	−4.29	3.35	4.29	5.51	1.03	5.32	76.87	4.02 × 10^{-10}	2.73 × 10^{-8}
Haloxylon	−3.20	3.88	3.20	2.63	0.20	3.40	20.57	5.18 × 10^{-10}	2.12 × 10^{-8}
Juniper	−4.24	3.36	4.24	5.35	0.97	5.21	90.45	4.46 × 10^{-10}	2.46 × 10^{-8}
Quercitin	−4.48	3.19	4.48	6.31	1.31	5.79	74.39	4.06 × 10^{-10}	2.70 × 10^{-8}
Rutin	−4.23	3.16	4.23	5.66	1.11	5.33	81.29	3.44 × 10^{-10}	3.20 × 10^{-8}

* All values are based on the present calculations.

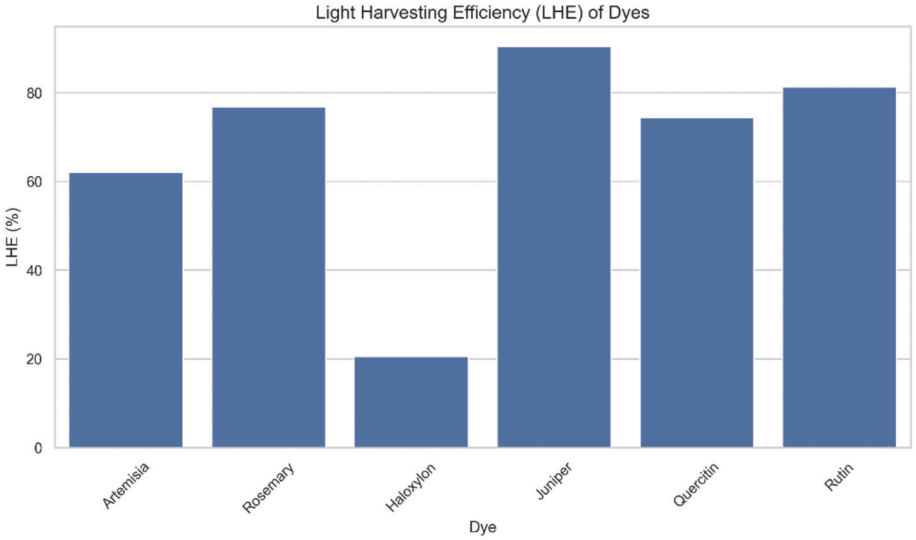

Fig. 9. Theoretically calculated light-harvesting efficiency (LHE) values for various investigated dyes. Calculations are made using CAM-B3LYP/6-311G(d,p) level of theory in methanol (CPCM).

dyes, that occurs within the range between the references, Quercitin and Rutin (4.48 eV > 4.29 eV > 4.23 eV). It is thus the most electron-withdrawing dye in the series, which provides stability in performance with limited efficiency in donating electrons within a DSSC. 3-(2-N-Acetyl-*N*-methylaminoethyl)indol has the lowest electronegativity for Haloxylon with χ = 3.20 eV, showing a higher tendency to donate electrons. The molecule thus potentially acts as a stronger sensitizer despite its lower stability.

Further exploration of performance traits is realized through the quantification of electron-donating and electron-accepting powers, ω^+ and ω^-, respectively. Haloxylon dye has the lowest value of ω^+, 3.40 eV, among the series. With also a quite low electron-accepting power, ω^- = 0.20 eV, this compound is a good electron acceptor making it a good stabilizer through effective electron withdrawal. Rosemary, represented by Scutellarein, strikes a balance of electron-donating and electron-accepting powers, both with highest values: ω^+ = 5.32 and ω^- = 1.03 eV, respectively. This makes it a viable candidate against the reference dyes Quercitin (ω^+ = 5.79 and ω^- = 1.31 eV), and Rutin (ω^+ = 5.33 and ω^- = 1.11 eV). Such a balance makes it a versatile co-sensitizer, capable of both electron donation and acceptance under appropriate conditions.

It is worth noting that Esculetin-6-O-glucoside and 3-p-Coumaroylquinic acid, from Artemisia and Juniper, respectively, exhibit values close to Rosemary and thus show similar behavior. For Esculetin-6-O-glucoside and 3-p-Coumaroylquinic acid, the ω^+ values respectively are 5.09 and 5.21 eV, while the ω^- values are 0.87 and 0.97 eV, in same respect. This highlights their similar behaviors in terms of stability and reactivity.

The electron donation and accepting powers complement the above analysis of light-harvesting efficiency and diffusion properties. The UV-absorbing dyes, Scutellarein, and 3-p-Coumaroylquinic acid, have stronger electron-accepting and electron-donating abilities and are hence suited for DSSC stabilizing. These dynamics, in turn, suggest that possible co-sensitization of these dyes with other good visible light sensitizers, may optimize both light absorption and stability toward a much more robust configuration.

Theoretically, the studied dyes provide protection mainly against UV radiation, while experimentally crude extracts are more suited for visible light absorption. Theoretical co-sensitization by the four dyes, with their experimental extract sensitization, would contribute to overall DSSC stability by reducing photo degradation under excessive UV exposure. This conclusion is consistent with the FT-IR spectra, electronic absorption spectra and TGA/DTA results, as the extracts exhibit high thermal stabilities with strong visible absorptions. The UV-protective complementary role of the proposed dyes is thus confirmed.

It is worth mentioning that combining multiple dyes for co-sensitization in DSSCs can introduce undesirable effects that may lower efficiency and stability [86]. Mainly, the key issues are summarized in a number of chemical behaviors. These include dye aggregation that hinders electron injection by π-π interactions, the spectral overlap that limits effective light harvesting, charge recombination that becomes more prevalent with the additional interfaces, and inconsistent anchoring that can lower electron injection efficiency. Energy level mismatch and dye desorption may also negatively affect performance, as do electrolyte incompatibility and the formation of degradation byproducts. A lack of synergistic effects between UV and visible/NIR-absorbing dyes can lead to minimal improvement or even lowered efficiency [87,88]. Thus, to optimize co-sensitization, it is essential to select dyes with complementary energy levels, stable anchoring and high absorption. Co-adsorbents or additives are needed to minimize recombination, stabilize dye attachment and prevent degradation [89]. To that extent, the present investigated dyes may add to the plate of available natural dyes ensuring co-sensitization applicability.

The theoretical findings here indicate that the proposed novel dyes from Rosemary Officinalis, Juniper Phoenicea, *Artemisia Campestris* and Haloxylon Scoparium (Scutellarein, 3-p-Coumaroylquinic acid, Esculetin-6-O-glucoside and 3-(2-N-Acetyl-*N*-methylaminoethyl)indol) have efficient UV absorption in the visible range combined with good photo-electrochemical capabilities. This makes the dyes suitable for sensitizers and UV protectors in DSSCs. On the other hand, experimental findings, specifically electronic absorption spectra, support the presence of possibly promising sensitizers that absorb in the visible range pointing to the presence of flavonoids, carotenoids and betalains in the mixture. These sensitizers can be used in co-sensitization with the theoretically investigated dyes (Scutellarein, 3-p-Coumaroylquinic acid, Esculetin-6-O-glucoside, 3-(2-N-Acetyl-*N*-methylaminoethyl)indol) to achieve higher stability and performance through UV light harvesting by the UV absorbers. In addition, thermal stabilities beyond 200 °C have been demonstrated by TG-DTA. The results encourage using the extracted systems in future production of new DSSCs. Theoretical testing of the new device efficiencies and stabilities will be strongly recommended.

It is worth noting that the dyes are potentially useful as UV filters and sunscreens in other applications [90]. For example, it is possible to use Esculetin-6-O-glucoside in certain sunscreen formulae owing to its

strong absorption in the lower UV range, as skin protectors. Scutellarein and 3-(2-N-Acetyl-*N*-methylaminoethyl)indol can be incorporated into various formulations to block UV radiation away from humans and in protecting other sensitive electronic devices [91]. Therefore, there is enough reason to expand the applications of such materials to DSSCs.

4.2.3. NBO analysis of electronic interactions

The NBO analysis is conducted to complement the HOMO-LUMO and TDDFT results by quantifying the internal electronic interactions and charge delocalization pathways within each dye. By identifying key donor-acceptor interactions and evaluating their stabilization energies (E(2)), it is possible to infer the degree of intramolecular charge transfer, a crucial factor for efficient sensitization. These insights are then correlated with the optical and electronic descriptors (f, ΔE_{LC}, *LHE*) to validate dye performance predictions.

As mentioned in Section 3.3, the Natural Bond Orbital (NBO) perturbation theory analysis provides deeper insights into the electronic interactions governing charge transfer in the studied dyes. These interactions are essential for evaluating the dye potential as DSSC sensitizer and UV absorber [79]. The results, summarized in Tables 4–9, highlight the top 5 most significant donor-acceptor interactions, which directly influence charge delocalization and molecular stability. By comparing the stabilization energies (E(2)) and electronic couplings (F(i,j)) among the selected phytochemicals and the reference dyes, a clear picture of their charge transfer properties and relative efficiency is established. The NBO analysis complements HOMO-LUMO gap considerations (Table 2) and TDDFT oscillator strengths (Table 1). This reinforces the rationalization of these dyes for DSSC applications by linking charge transfer efficiency with their optoelectronic properties.

As depicted by the molecular structures, in Fig. 2 **A**, the electronic delocalization in Esculetin-6-O-glucoside (*Artemisia Campestris*) is driven by its extended π-conjugation and hydroxyl functional groups, facilitating charge redistribution. This is evidenced by the O3 LP(π) - O8-C22 BD*(π*) interaction, which stabilizes at 48.10 kcal/mol (Table 4), suggesting efficient charge movement across the molecule. However, its relatively large HOMO-LUMO gap (7.00 eV, Table 2) limits its visible-light absorption, positioning it more as a UV protector rather than a standalone sensitizer. Despite its strong donor-acceptor interactions, the minimal overlap with the visible spectrum indicates its primary role in UV shielding rather than direct electron injection into TiO_2. On the other hand, the high stabilization energy supports its use in co-sensitization strategies where UV absorption is needed alongside a strong visible-light sensitizer. In contrast, Scutellarein (*Rosmarinus Officinalis*) (Fig. 2 **B**) exhibits a more extended conjugation system, leading to higher charge delocalization than Esculetin-6-O-glucoside. The C32-C33 BD(π) - C26-C28 BD*(π*) interaction stabilizes at 39.92 kcal/mol (Table 5), complemented by the O1 LP(π) - C20-C22 BD*(π*) interaction at 39.64 kcal/mol (Table 5). These electronic interactions facilitate improved charge mobility, enhancing its function as a sensitizer. A higher oscillator strength ($f = 0.64$, Table 1) and a relatively smaller HOMO-LUMO gap (6.69 eV, Table 2) further indicate its ability to efficiently absorb in the UV–Vis regions. Compared to Quercetin, which displays O10 LP(π) - C7-C9 BD*(π*) at E(2) = 26.62 kcal/mol (Table 8), Scutellarein exhibits stronger donor-acceptor stabilization, reinforcing its potential as an efficient sensitizer with dual absorption in UV and visible regions. The alignment of its LUMO level with the TiO_2 conduction band (Table 2) further supports its viability as a DSSC sensitizer.

Expanding on these trends, the strongest electronic interactions among the studied dyes are observed in 3-p-Coumaroylquinic acid (*Juniperus Phoenicea*) (Fig. 2 **D**), where the O1 LP(π) - C2-O4 BD*(π*) interaction stabilizes at 54.77 kcal/mol (Table 7). An additional strong stabilization at O19 LP(π) - C15-O20 BD*(π*) is also observed at 54.32 kcal/mol (Table 7). The presence of hydroxyl (-OH) and carboxyl (-COOH) groups enhances its binding affinity to TiO_2, ensuring effective electron transport. These stabilization energies exceed those observed in Quercetin and Rutin (Tables 8–9) and (Figs. 2 ***E*-F**), emphasizing its superior performance in DSSCs. A high oscillator strength ($f = 1.02$, Table 1) aligns with this observation, indicating that 3-p-Coumaroylquinic acid functions as a highly effective primary sensitizer with additional UV protection benefits. The overlap, of its excitation energies (Table 1) with the visible spectrum and its optimized frontier molecular orbitals, suggests a strong electron injection efficiency into TiO_2. Unlike the oxygen-based charge delocalization observed in the previous dyes, 3-(2-N-Acetyl-*N*-methylaminoethyl)indol (Haloxylon Scoparium) (Fig. 2 **C**) operates through nitrogen-centered interactions. The N3 LP(σ) - C5-C9 BD*(π*) and N3 LP(σ) - C7-C8 BD*(π*) interactions (Table 6), with stabilization energies of 36.74 kcal/mol and 35.79 kcal/mol, respectively, suggest moderate charge delocalization. However, the presence of a relatively high *LUMO* level (0.68 eV, Table 2) and a low oscillator strength ($f = 0.10$, Table 1) limits its efficiency as a primary sensitizer. Instead of being a direct sensitizer, Haloxylon charge retention properties may contribute to minimizing recombination losses when paired with stronger dyes. Moreover, its limited visible-light absorption suggests that it plays a secondary role rather than serving as a dominant DSSC dye.

A comparative assessment with the reference dyes Quercetin and Rutin confirms that the investigated phytochemicals generally exhibit stronger electronic interactions. Quercetin, a well-established DSSC sensitizer, presents moderate stabilization energies, including O10 LP(π) - C7-C9 BD*(π*) at 26.62 kcal/mol (Table 8). On the other hand, Rutin displays significantly weaker donor-acceptor interactions (O12 LP(σ) - C34 RY*(1), E(2) = 8.65 kcal/mol (Table 9)), which can be attributed to the presence of an additional glycosyl unit that disrupts its conjugation, (Fig. 2 **F**). This lower electronic coupling explains its lowered DSSC efficiency (0.71 %) compared to Quercetin (2.15 %), as described earlier [19]. While the observed correlation between stabilization energies and DSSC efficiency is compelling, other factors, including dye aggregation, anchoring efficiency and electrolyte interactions, also contribute to overall device performance. The insights derived from NBO perturbation theory align well with previous electronic structure analyses, including HOMO-LUMO calculations (Table 2) and TDDFT results (Table 1), where high oscillator strengths and favorable charge transport properties were observed. Fig. 10 summarizes key performance descriptors such as stabilization energy, oscillator strength, injection driving force (ΔE_{LC}) and *LHE* as a heatmap. The Figure clearly highlights Juniper as the most promising candidate across all evaluated metrics, while Haloxylon remains an outlier with generally weaker photovoltaic indicators. 3-p-Coumaroylquinic acid from *Juniperus phoenicea* shows the highest E(2) stabilization energy (54.77 kcal/mol), corresponding to intense π-conjugation and lone-pair resonance. This correlates with its

Table 4
Second Order Perturbation Theory Analysis of Fock Matrix in NBO Basis for Artemisia.

Dye	Donor	Type	Occupancy	Acceptor	Type.1	Occupancy	E(2) kcal/Mol	E(j)-E(i) a.u.	F(i,j) a.u.
	O3	LP (π)	2.00	O8-C22	BD* (π*)	1.99	48.10	0.45	0.13
	O8	LP (π)	2.00	O3-C22	BD* (σ*)	1.99	40.99	0.71	0.15
Artemisia	O3	LP (π)	2.00	C16-C17	BD* (π*)	1.97	31.80	0.45	0.11
	C18-C20	BD (π)	1.97	C16-C17	BD* (π*)	1.97	31.49	0.37	0.10
	C16-C17	BD (π)	1.97	C12-C19	BD* (π*)	1.97	31.25	0.37	0.10

Table 5
Second Order Perturbation Theory Analysis of Fock Matrix in NBO Basis for Rosemary.

Dye	Donor	Type	Occupancy	Acceptor	Type.1	Occupancy	E(2) kcal/Mol	E(j)-E(i) a.u.	F(i,j) a.u.
	C32-C33	BD (π)	1.98	C26-C28	BD* (π*)	1.97	39.92	0.36	0.11
	O1	LP (π)	2.00	C20-C22	BD* (π*)	1.98	39.64	0.47	0.12
Rosemary	C14-C16	BD (π)	1.97	C15-C18	BD* (π*)	1.97	36.64	0.37	0.10
	O11	LP (π)	2.00	C32-C33	BD* (π*)	1.98	36.21	0.44	0.12
	O5	LP (π)	2.00	C14-C16	BD* (π*)	1.97	34.90	0.42	0.12

Table 6
Second Order Perturbation Theory Analysis of Fock Matrix in NBO Basis for Haloxylon.

Dye	Donor	Type	Occupancy	Acceptor	Type.1	Occupancy	E(2) kcal/Mol	E(j)-E(i) a.u.	F(i,j) a.u.
	N3	LP (σ)	2.00	C5-C9	BD* (π*)	1.98	36.74	0.33	0.10
	N3	LP (σ)	2.00	C7-C8	BD* (π*)	1.97	35.79	0.32	0.10
Haloxylon	C7-C8	BD (π)	1.97	C11-C15	BD* (π*)	1.98	24.55	0.29	0.08
	C7-C8	BD (π)	1.97	C10-C13	BD* (π*)	1.99	24.17	0.30	0.08
	C10-C13	BD (π)	1.99	C11-C15	BD* (π*)	1.98	24.01	0.30	0.08

Table 7
Second Order Perturbation Theory Analysis of Fock Matrix in NBO Basis for Juniper.

Dye	Donor	Type	Occupancy	Acceptor	Type.1	Occupancy	E(2) kcal/Mol	E(j)-E(i) a.u.	F(i,j) a.u.
	O1	LP (π)	2.00	C2-O4	BD* (π*)	2.00	54.77	0.44	0.14
	O19	LP (π)	2.00	C15-O20	BD* (π*)	2.00	54.32	0.45	0.14
Juniper	O20	LP (π)	2.00	C15-O19	BD* (σ*)	1.99	39.11	0.73	0.15
	C9-C11	BD (π)	1.98	C6-C7	BD* (π*)	1.97	37.76	0.37	0.11
	O12	LP (π)	2.00	C9-C11	BD* (π*)	1.98	36.09	0.45	0.12

Table 8
Second Order Perturbation Theory Analysis of Fock Matrix in NBO Basis for Quercetin.

Dye	Donor	Type	Occupancy	Acceptor	Type.1	Occupancy	E(2) kcal/Mol	E(j)-E(i) a.u.	F(i,j) a.u.
	O10	LP (π)	2.00	C7-C9	BD* (π*)	1.98	26.62	0.48	0.10
	C7-C9	BD (π)	1.98	C1-O26	BD* (π*)	1.99	25.79	0.39	0.09
Quercetin	C5-C6	BD (π)	1.98	C1-O26	BD* (π*)	1.99	25.57	0.38	0.09
	O20	LP (π)	2.00	C12-C13	BD* (π*)	1.98	24.53	0.47	0.10
	O22	LP (π)	2.00	C11-C15	BD* (π*)	1.98	24.50	0.46	0.10

Table 9
Second Order Perturbation Theory Analysis of Fock Matrix in NBO Basis for Rutin.

Dye	Donor	Type	Occupancy	Acceptor	Type.1	Occupancy	E(2) kcal/Mol	E(j)-E(i) a.u.	F(i,j) a.u.
	O12	LP (σ)	2.00	C34	RY* (1)	2.00	8.65	1.72	0.110
	O12	LP (π)	2.00	C34	RY* (1)	2.00	4.40	1.52	0.075
Rutin	O5-H69	BD (σ)	1.99	C22	RY* (1)	2.00	3.85	1.64	0.071
	O8	LP (σ)	2.00	C24	RY* (1)	2.00	3.69	1.69	0.071
	O13	LP (σ)	2.00	C38	RY* (1)	2.00	3.39	1.84	0.071

highest oscillator strength ($f = 1.02$), low ΔE_{LC} value (3.12 eV), and superior light-harvesting efficiency ($LHE = 90.45$ %). Similarly, Scutellarein (Rosemary) exhibits strong π-π* interactions with E(2) values around 39–40 kcal/mol, aligned with its favorable HOMO-LUMO alignment ($\Delta E_{LC} = 3.05$ eV) and LHE (76.87 %). These trends suggest that stabilization energies from NBO analysis can serve as indirect indicators of charge-transfer efficiency and electronic performance in DSSC dyes. In contrast, Haloxylon's 3-(2-N-Acetyl-*N*-methylaminoethyl) indol, while exhibiting moderate stabilization energies (35–36 kcal/mol), has a high ΔE_{LC} (4.68 eV) and very low LHE (20.57 %), indicating poor sensitization potential despite internal electron donation. This supports the conclusion that strong NBO stabilization is necessary but not sufficient for good photovoltaic behavior. It must also align with proper orbital energy levels and absorption intensity.

5. Conclusion

Natural dyes from four globally recognized plants, *Artemisia campestris*, *Rosmarinus officinalis*, Haloxylon scoparium, Haloxylon scoparium and *Juniperus phoenicea*, are collected from north Algeria in North Africa, and are studied here. The low-cost and ecofriendly phytochemicals are comparatively assessed as possible future consideration as sensitizers and UV protectors in dye sensitized solar cells, for the first time. Experimentally, the plant extracts are thermally stabile beyond

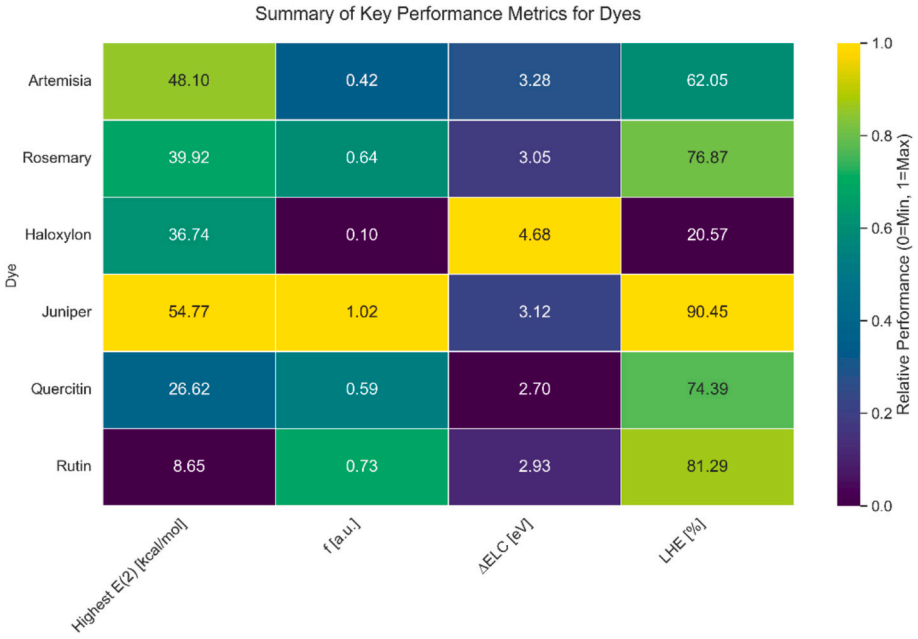

Fig. 10. Heatmap summarizing key performance descriptors for various investigated dyes. Calculations are made using the CAM-B3LYP/6-311G(d,p) level in methanol (CPCM).

200 °C, and have functional groups -OH and -COOH with conjugated π-systems. The extracts exhibit broad absorption ranges spanning both UV and visible ranges (190 to 800 nm), indicating their suitability as co-sensitizers. Theoretically, DFT and TDDFT are used to assess UV absorption, electronic features and stability of phytochemicals Esculetin-6-O-glucoside, Scutellarein, 3-(2-N-Acetyl-*N*-methylaminoethyl)indol and 3-p-Coumaroylquinic acid, corresponding to the plants. The results demonstrate efficient light harvesting in both the UV and visible ranges, with some phytochemicals exhibiting strong UV absorption properties. Comparisons with the reference dyes Quercetin and Rutin indicate favorable electrochemical properties for DSSC applications. NBO perturbation analysis further reveals key donor-acceptor interactions and stabilization energies, reinforcing charge transfer efficiency. Notably, 3-p-Coumaroylquinic acid (Juniperus) exhibits the highest stabilization energy E(2) = 54.77 kcal/mol, confirming its role as a primary sensitizer. Scutellarein (Rosemary) shows strong π-conjugation and charge delocalization, enhancing its dual functionality. Esculetin-6-O-glucoside (Artemisia) demonstrates superior UV absorption properties, making it more suitable for protection than direct sensitization. 3-(2-N-Acetyl-*N*-methylaminoethyl)indol (Haloxylon) plays a stabilizing role rather than serving as an efficient charge transporter. The integration of NBO perturbation theory with TDDFT results enable a deeper understanding of charge-transfer mechanisms and stability factors in the investigated phytochemicals. Notably, 3-p-Coumaroylquinic acid (Juniperus) and Scutellarein (Rosemary) exhibit the highest stabilization energies and oscillator strengths, correlating with superior light harvesting energy and energy-level alignment with TiO_2. These findings are supported by comparative benchmarking with Quercetin and Rutin, and help validate the computational screening approach. The study effectively bridges experimental trends (for the extracts) with theoretical predictions (for corresponding phytochemicals) offering valuable guidance for isolation and co-sensitization in future DSSC manufacturing.

CRediT authorship contribution statement

Mohammed Madani Taouti: Writing – original draft, Software, Methodology, Investigation. **Ali Cheknane:** Writing – review & editing, Supervision, Resources, Project administration, Conceptualization. **Naceur Selmane:** Writing – review & editing, Validation, Supervision, Conceptualization. **Noureddine Benaya:** Investigation. **Hikmat S. Hilal:** Writing – review & editing, Supervision.

Declaration of competing interest

The authors declare that they have no known competing financial interests or personal relationships that could have appeared to influence the work reported in this paper.

Acknowledgment

A. C., N. S. and M. M. T. thank Amar Telidji University, Laghouat, financial support through the PRFU Project/N° A10N01UN030120220002: “Contribution à l’étude des propriétés physico-chimiques des nouveaux matériaux: Applications dans le domaine des énergies renouvelables”. Thanks are also due to “La Direction Générale de la Recherche Scientifique et du Développement Technologique (DGRSDT)”. We also, thank the “Plateau Technique d’Analyses Physico-Chimiques (PTAPC-CRAPC)-LAGHOUAT-Algeria”, and the “Laboratory of Physical Chemistry of Materials (LPCM), Faculty of Sciences (UATL), Laghouat, Algeria”, for providing access and guidance with the characterization equipment. H. S. H. thanks An-Najah National University for technical and logistic support.

Data availability

Original data will be made available after publication on sound demand.

References

[1] C.J. Rhodes, Solar energy: principles and possibilities, Sci. Prog. 93 (1) (2010) 37–112.
[2] M. Grätzel, Dye-sensitized solar cells, J. Photochem. Photobiol. C Photchem. Rev. 4 (2) (2003) 145–153.
[3] A. Hagfeldt, G. Boschloo, L. Sun, L. Kloo, H. Pettersson, Dye-sensitized solar cells, Chem. Rev. 110 (11) (2010) 6595–6663.
[4] A.W. Copeland, O.D. Black, A. Garrett, The photovoltaic effect, Chem. Rev. 31 (1) (1942) 177–226.

[5] M.S. Ahmad, A.K. Pandey, N. Abd Rahim, Advancements in the development of TiO2 photoanodes and its fabrication methods for dye sensitized solar cell (DSSC) applications. A review, Renew. Sustain. Energy Rev. 77 (2017) 89–108.

[6] A. Omar, M.S. Ali, N. Abd Rahim, Electron transport properties analysis of titanium dioxide dye-sensitized solar cells (TiO2-DSSCs) based natural dyes using electrochemical impedance spectroscopy concept: a review, Solar Energy 207 (2020) 1088–1121.

[7] V. Nunes, F. Lima, E. Teixeira, P. Maia Júnior, A. Almeida, F. Freire, Synthesis of TiO2/ZnO photoanodes on FTO conductive glass for photovoltaic applications, Ceramica 69 (2023) 79–86.

[8] R. Baby, P.D. Nixon, N.M. Kumar, M. Subathra, N. Ananthi, A comprehensive review of dye-sensitized solar cell optimal fabrication conditions, natural dye selection, and application-based future perspectives, Environ. Sci. Pollut. Res. 29 (2022) 1–34, https://doi.org/10.1007/s11356-021-16976-8.

[9] S.-H. Rahman, Abdul-Siddiq, Muhammad-Hussain, Muhammad-Khalid-Qamar, Samina-Hameed, Safia-Waris, Muhammad, "research on dye sensitized solar cells: recent advancement toward the various constituents of dye sensitized solar cells for efficiency enhancement and future prospects,", RSC Adv. 13 (28) (2023) 19508–19529.

[10] B. O'regan, M. Grätzel, A low-cost, high-efficiency solar cell based on dye-sensitized colloidal TiO2 films, nature 353 (6346) (1991) 737–740.

[11] J.A. Castillo-Robles, E. Rocha-Rangel, J.A. Ramírez-de-León, F.C. Caballero-Rico, E.N. Armendáriz-Mireles, Advances on dye-sensitized solar cells (DSSCs) nanostructures and natural colorants: a review, J. Compos. Sci. 5 (11) (2021) 288.

[12] B.K. Korir, J.K. Kibet, S.M. Ngari, A review on the current status of dye-sensitized solar cells: toward sustainable energy, Energy Sci. Eng. 12 (8) (2024) 3188–3226.

[13] M.M. Taouti, N. Selmane, A. Cheknane, H.S. Hilal, Improved efficiency and stability for acridine orange sensitizers by adding electron donating/accepting π-linker moieties, Computational and Theoretical Chemistry 1234 (2024) 114550, https://doi.org/10.1016/j.comptc.2024.114550.

[14] G.F.C. Mejica, R. Ramaraj, Y. Unpaprom, Natural dye (chlorophyll, anthocyanin, carotenoid, flavonoid) photosensitizer for dye-sensitized solar cell: a review, Maejo International Journal of Energy and Environmental Communication 4 (1) (2022) 12–22.

[15] W. Shah, S.M. Faraz, Z.H. Awan, Photovoltaic properties and impedance spectroscopy of dye sensitized solar cells co-sensitized by natural dyes, Phys. B Condens. Matter 654 (2023) 414716.

[16] S. Kaliramna, S.S. Dhayal, R. Chaudhary, S. Khaturia, K.L. Ameta, N. Kumar, A review and comparative analysis of different types of dyes for applications in dye-sensitized solar cells, Braz. J. Phys. 52 (4) (2022) 136.

[17] A.M. Lazić, L.R. Matović, N.P. Trišović, N.V. Valentić, Harnessing the potential of selected plant pigments in dye-sensitized solar cells: the current status, Hem. Ind. 79 (1) (2025) 47–65.

[18] I.-U. Fierascu, Camelia-Avramescu, Sorin-Marius-Cimpeanu, Carmen-Georgescu, Mihaela-Ioana-Fierascu, Radu-Claudiu-Ortan, Alina-Sutan, Anca-Nicoleta-Anuta, Valentina-Zanfirescu, Anca, Genoprotective, antioxidant, antifungal and anti-inflammatory evaluation of hydroalcoholic extract of wild-growing *Juniperus communis* L.(Cupressaceae) native to Romanian southern sub-Carpathian hills, BMC Complement. Altern. Med. 18 (2018) 1–14.

[19] D. Zhao, Q. Lu, R. Su, Y. Li, M. Zhao, Light harvesting and optical-electronic properties of two quercitin and rutin natural dyes, Appl. Sci. 9 (12) (2019) 2567.

[20] J. Ramirez-Perez, C. Maria, C.P. Santacruz, Impact of solvents on the extraction and purification of vegetable dyes onto the efficiency for dye-sensitized solar cells, Renewables: Wind, Water, and Solar 6 (1) (2019) 1, https://doi.org/10.1186/s40807-019-0055-x.

[21] N.-J.P. Downs, Alfio-V. Galligan, Linda Turner, Joanna Amar, Abdurazaq King, Rachel Ultra, Filipina Butler, Harry J., Solar radiation and the UV index: an application of numerical integration, trigonometric functions, online education and the modelling process, Int. J. Res. Educ. Sci. 2 (2015) 179–189.

[22] M.-K. Son, H. Seo, Effect of ultraviolet radiation on the long-term stability of dye-sensitized solar cells, Electron. Mater. Lett. 16 (6) (2020) 556–563, https://doi.org/10.1007/s13391-020-00249-6.

[23] C. Dawo, M.A. Afroz, P.K. Iyer, H. Chaturvedi, Effect of UV-ozone exposure on the dye-sensitized solar cells performance, Sol. Energy 208 (2020) 212–219, https://doi.org/10.1016/j.solener.2020.07.064.

[24] F.-M. Kabir, Md-Mossaraf-Hossain-Aftab Serajum-Bhuiyan, Hamidreza-Hasani Sikandar-Ghanbari, Mirette-De-Silva Amirhossein-Fawzy, G.L. Thushani, M.R.A. Mohammadzadeh Ribwar, Instability of dye-sensitized solar cells using natural dyes and approaches to improving stability–an overview, Sustain Energy Technol Assess 52 (2022) 102196.

[25] S.H. Sumrra, A.U. Hassan, W. Zafar, Z.H. Chohan, K.A. Alrashidi, Molecular engineering for UV-vis to NIR absorption/emission bands of pyrazine-based A-π-D-π-a switches to design TiO2 tuned dyes: DFT insights, J. Fluoresc. (2024) 1, https://doi.org/10.1007/s10895-024-03891-7.

[26] S. Tahmasebi, Z. Tavangar, M. Hamadanian, Using of *Artemesia absinthinum*, *Verbascum thapsus*, *Viola odorata*, *Matricaria chamomilla* and *Coriandrum sativum* natural dyes in making dye-sensitized solar cells, Advanced Materials and New Coatings 8 (32) (2020) 2346–2356.

[27] S. Das, S. Roy Maulik, Recent approaches and advancements in natural dyes, in: Natural Dyes and Sustainability, 2024, pp. 63–78, https://doi.org/10.1007/978-3-031-47471-2_4.

[28] A. Listorti, B. O'Regan, J.R. Durrant, Electron transfer dynamics in dye-sensitized solar cells, Chem. Mater. 23 (15) (2011) 3381–3399, https://doi.org/10.1021/cm200651e.

[29] I.O. Oladele, B. Abiodun Makinde-Isola, N.I. Agbeboh, B.O. Iwarere, Thermal stability, moisture uptake potentials and mechanical properties of modified plant based cellulosic fiber-animal wastes hybrid reinforced epoxy composites, Journal of Natural Fibers 19 (12) (2022) 4427–4442.

[30] J. Ferguson, Z. Petrovic, Thermal stability of segmented polyurethanes, Eur. Polym. J. 12 (3) (1976) 177–181.

[31] W.-S. Zahnit, Lazhar-Bensouici Ouanissa-Bechki, Mohammed-Benchikha Chawki-Messaoudi, Imane-Awuchi Naima-Larkem, Barbara-Simal-Gandara Chinaza-Godswill-Sawicka, Jesus, Phytochemical profiling, mineral elements, and biological activities of Artemisia campestris L. grown in Algeria, Horticulturae 8 (10) (2022) 914 [Online]. Available: https://www.mdpi.com/2311-7524/8/10/914.

[32] Y.-M. Amar, Irene Boumediene-Bonacorsi, Gregorio Costa, Gaetana Pezzino, Antonina Saija, Mariateresa Cristani, Soulef Boussahel, Guido Ferlazzo, Aicha Meddah, Tirtouil, Phytochemicals, antioxidant and antiproliferative properties of *Rosmarinus officinalis* L on U937 and CaCo-2 cells, Iranian Journal of Pharmaceutical Research: IJPR 16 (1) (2017) 315.

[33] S. Haida, A. Kribii, Chemical composition, phenolic content and antioxidant capacity of *Haloxylon scoparium* extracts, S. Afr. J. Bot. 131 (2020) 151–160.

[34] D.-R. Ghouti, Wahiba-Abdallah, Moussaoui-Pires, Tânia-CSP-Calhelha, Ricardo-C-Alves, Maria-José-Abderrahmane, Lazzouni-Hamadi-Barros, Lillian-Ferreira, Isabel-CFR, Phenolic profile and in vitro bioactive potential of Saharan *Juniperus phoenicea* L. and *Cotula cinerea* (Del) growing in Algeria, Food Funct. 9 (9) (2018) 4664–4672.

[35] A.E.-H.H. Mohamed, M. El-Sayed, M.E. Hegazy, S.E. Helaly, A.M. Esmail, N. S. Mohamed, Chemical constituents and biological activities of *Artemisia herba-alba*, Rec. Nat. Prod. 4 (1) (2010).

[36] B. Jamshidi, A. Etminan, A. Mehrabi, L. Shooshtari, A. Pour-Aboughadareh, Comparison of phytochemical properties and expressional profiling of artemisinin synthesis-related genes in various Artemisia species, Heliyon 10 (5) (2024) e26388, https://doi.org/10.1016/j.heliyon.2024.e26388.

[37] S. Dogra, B. Koul, J. Singh, M. Mishra, D. Yadav, Phytochemical analysis, antimicrobial screening and in vitro pharmacological activity of *Artemisia vestita* leaf extract, Molecules 29 (8) (2024) 1829.

[38] N. Hendel, D. Sarri, M. Sarri, E. Napoli, A. Palumbo Piccionello, G. Ruberto, Phytochemical analysis and antioxidant and antifungal activities of powders, methanol extracts, and essential oils from Rosmarinus officinalis L. and Thymus ciliatus Desf. Benth, Int. J. Mol. Sci. 25 (14) (2024) 7989.

[39] P. Hohenberg, W. Kohn, Inhomogeneous electron gas, Phys. Rev. 136 (3B) (1964) B864.

[40] E. Runge, E.K. Gross, Density-functional theory for time-dependent systems, Phys. Rev. Lett. 52 (12) (1984) 997.

[41] J.-D. Chai, M. Head-Gordon, Long-range corrected double-hybrid density functionals, J. Chem. Phys. 131 (17) (2009) 174105, https://doi.org/10.1063/1.3244209.

[42] M. Kaupp, A. Wodyński, A.V. Arbuznikov, S. Fürst, C.J. Schattenberg, Toward the next generation of density functionals: escaping the zero-sum game by using the exact-exchange energy density, Acc. Chem. Res. 57 (13) (2024) 1815–1826.

[43] F. Neese, The ORCA program system, Wiley Interdiscip. Rev.: Comput. Mol. Sci. 2 (1) (2012) 73–78.

[44] F. Neese, Software update: the ORCA program system—version 5.0, WIREs Comput. Mol. Sci. 12 (5) (2022) e1606.

[45] A.E. Reed, L.A. Curtiss, F. Weinhold, Intermolecular interactions from a natural bond orbital, donor-acceptor viewpoint, Chem. Rev. 88 (6) (1988) 899–926.

[46] E.D. Glendening, C.R. Landis, F. Weinhold, Natural bond orbital methods, WIREs Comput. Mol. Sci. 2 (1) (2012) 1–42.

[47] M.-K.-P. Hossain, M. Firoz-Mia, M.N.H. Mortuza, A.A. Rahaman, M.S. Karim, M. R. Islam, Jahid M.M. Ahmed, Farid Khan, A. Mubarak, Effect of dye extracting solvents and sensitization time on photovoltaic performance of natural dye sensitized solar cells, Results Phys. 7 (2017) 1516–1523.

[48] S.S. Malhotra, M. Ahmed, M.K. Gupta, A. Ansari, Metal-free and natural dye sensitized solar cells: recent advancement and future perspectives, Sustainable Energy Fuels 8 (2024) 4127–4163.

[49] T. Daniel, L. Rhyman, P. Ramasami, Exploring the efficiency of C343 coumarin dye-sensitized solar cells using substituents, Chem. A Eur. J. 128 (2024) 7795–7803, https://doi.org/10.1021/acs.jpca.4c03300.

[50] L. Zhang, J.M. Cole, Anchoring groups for dye-sensitized solar cells, ACS Appl. Mater. Interfaces 7 (6) (2015) 3427–3455.

[51] S. Fatima, A. Mansha, S. Asim, A. Shahzad, Absorption spectra of coumarin and its derivatives, Chem. Pap. 76 (2) (2022) 627–638, https://doi.org/10.1007/s11696-021-01902-6.

[52] B.C. Mphande, A. Pogrebnoi, Impact of extraction methods upon light absorbance of natural organic dyes for dye sensitized solar cells application, J. Energy Nat. Resour. 3 (3) (2014) 38–45.

[53] T.-C. Belwal, Christian-Prieto, M.A. Venskutonis, Petras-Rimantas Daglia, Maria Devkota, Hari-Prasad Baldi, Alessandra, Shahira Ezzat, Mohammed, L.-S. Gómez-Gómez, Maha Mahmoud, Effects of different drying techniques on the quality and bioactive compounds of plant-based products: a critical review on current trends, Drying Technol. 40 (8) (2022) 1539–1561.

[54] N. Alsaud, M. Farid, Insight into the influence of grinding on the extraction efficiency of selected bioactive compounds from various plant leaves, Appl. Sci. 10 (18) (2020) 6362.

[55] W. Wu, Y. Li, J. Zhang, X. Guo, L. Wang, H. Ågren, Theoretical modelling of metal-based and metal-free dye sensitizers for efficient dye-sensitized solar cells: a review, Solar Energy 277 (2024) 112748.

[56] J. Conradie, Effective dyes for DSSCs–important experimental and calculated parameters, Energy Nexus 13 (2024) 100282.

[57] M.R.S.A. Janjua, Photovoltaic properties and enhancement in near-infrared light absorption capabilities of acceptor materials for organic solar cell applications: a quantum chemical perspective via DFT, J. Phys. Chem. Solids 171 (2022) 110996, https://doi.org/10.1016/j.jpcs.2022.110996.
[58] G. Maheswari, R.V. Williams, FT-IR, UV, molecular structure, MESP, NBO, HOMO-LUMO investigation and modeling of oligomers of polyvinyl alcohol for dye-sensitized solar cell application: a DFT approach, IJRAR 6 (2019) 513–528 [Online]. Available: ijrar.org/papers/19K1072.pdf.
[59] J.M. Juma, S.A.H. Vuai, N.S. Babu, TD-DFT investigations on optoelectronic properties of fluorescein dye derivatives in dye-sensitized solar cells (DSSCs), International Journal of Photoenergy 2019 (2019) 1–8, https://doi.org/10.1155/2019/4616198.
[60] S.J. Sharma, N. Sekar, Exploring charge transfer effects on linear, non-linear optical, and dye-sensitized solar cell properties: a DFT and TD-DFT investigation of carbazole and aniline-based dyes, Int. J. Quantum Chem. 124 (13) (2024) e27419.
[61] M. Hussain, T. Jalali, L. Maftoon-Azad, S. Osfouri, Performance evaluation of natural dye-sensitized solar cells: a comparison of density functional theory and experimental data on chlorophyll, anthocyanin, and cocktail dyes as sensitizers, ACS Appl. Electron. Mater. 6 (3) (2024) 1693–1709.
[62] M. Soroush, K.K.S. Lau, Insights Into Dye-Sensitized Solar Cells From Macroscopic-Scale First-Principles Mathematical Modeling, in: Dye-Sensitized Solar Cells, 2019, pp. 83–119.
[63] C.I. Oprea, M.A. Girtu, Structure and electronic properties of TiO(2) nanoclusters and dye(−)nanocluster systems appropriate to model hybrid photovoltaic or photocatalytic applications, Nanomaterials (Basel) 9 (3) (2019), https://doi.org/10.3390/nano9030357.
[64] J.M. Cole, Y. Gong, J. McCree-Grey, P.J. Evans, S.A. Holt, Modulation of N3 and N719 dye···TiO2 interfacial structures in dye-sensitized solar cells as influenced by dye counter ions, dye deprotonation levels, and sensitizing solvent, ACS Appl Energy Mater 1 (6) (2018) 2821–2831, https://doi.org/10.1021/acsaem.8b00464.
[65] B. Maldon, N. Thamwattana, "review of diffusion models for charge-carrier densities in dye-sensitized solar cells," *journal of physics*, Communications 4 (8) (2020) 082001, https://doi.org/10.1088/2399-6528/abacd6.
[66] A. Majid, S. Kiran, Q.u.A. Sandhu, S. Khan, S. Khan, The effects of polar solvents on structural, electronic, and optical properties of organic dyes, Int. J. Quantum Chem. 122 (9) (2022) e26876, https://doi.org/10.1002/qua.26876.
[67] M.R.S.A. Janjua, All-small-molecule organic solar cells with high fill factor and enhanced open-circuit voltage with 18.25% PCE: physical insights from quantum chemical calculations, Spectrochim. Acta A Mol. Biomol. Spectrosc. 279 (2022) 121487, https://doi.org/10.1016/j.saa.2022.121487.
[68] T.-M. Daeneke, Attila-J-Uemura, Yu-makuta, Satoshi-Fekete, Monika-Tachibana, Yasuhiro-Koumura, Nagatoshi-Bach, udo-Spiccia, Leone, "dye regeneration kinetics in dye-sensitized solar cells,", J. Am. Chem. Soc. 134 (41) (2012) 16925–16928.
[69] R.-F. Katoh, Akihiro Yoshihara, Toshitada Hara, Kohjiro Fujihashi, Gaku Takano, Shingo Murata, Shigeo Arakawa, Hironori Tachiya, M, Efficiencies of electron injection from excited N3 dye into nanocrystalline semiconductor (ZrO2, TiO2, ZnO, Nb2O5, SnO2, In2O3) films, J. Phys. Chem. B. 108 (15) (2004) 4818–4822.
[70] F. Arkan, F. Pakravesh, F. Barati Darband, S. Sabagh, M. Izadyar, Recent progress toward high-performance dye-sensitized solar cells: a review, J. Iran. Chem. Soc. 21 (3) (2024) 577–638.
[71] Y. Sekkat, A. Fitri, O. Britel, A.T. Benjelloun, M. Mcharfi, M. Benzakour, DFT/TDDFT investigation of the effect of Electron acceptor groups on photovoltaic performance using phenothiazine-based D-ai-π-A dyes for DSSC applications, ChemistrySelect 9 (36) (2024) e202403042.
[72] T. Ranwaha, I. Elegbeleye, N. Maluta, R. Maphanga, Optical and electronic properties of croconates dye molecules adsorbed on TiO2 brookite nanocluster for dye sensitized solar cells application, Mater. Express 10 (11) (2020) 1917–1924, https://doi.org/10.1166/mex.2020.1848.
[73] N. Drigo, Molecular Engineering of Functional Materials for Optoelectronic Applications, EPFL, 2020.
[74] J.L. Gázquez, A. Cedillo, A. Vela, Electrodonating and Electroaccepting powers, Chem. A Eur. J. 111 (10) (2007) 1966–1970, https://doi.org/10.1021/jp065459f.
[75] L. Naik, I.A.M. Khazi, G. Malimath, Studies on photosensitization of TiO2 nanoparticles by novel 1, 3, 4-oxadiazoles derivatives, Optik 183 (2019) 732–741, https://doi.org/10.1016/j.ijleo.2019.02.145.
[76] L.-C.C. Coetzee, A.S. Adeyinka, N. Magwa, A theoretical evaluation of the efficiencies of metal-free 1,3,4-oxadiazole dye-sensitized solar cells: insights from electron–hole separation distance analysis, Energies 15 (13) (2022) 4913, https://doi.org/10.3390/en15134913.
[77] A.-U.-S. Hassan, Sajjad-H Mustafa, Ghulam Noreen, Sadaf Ali, Asad Sara, Syeda Imran, Muhammad, Enhancing NLO performance by utilizing tyrian purple dye as donor moiety in organic DSSCs with end capped acceptors: a theoretical study, J. Mol. Graph. Model. 124 (2023) 108538.
[78] N.M. Malashi, Y.A.C. Jande, N. Wazzan, Z. Safi, O.S. Al-Qurashi, R. Costa, Chemical structure modification of brazilin-based natural dye with TiO2 nanostructure improves photovoltaic properties for maximum simulated PCE for DSSCs application, Mater Today Commun 40 (2024) 109756.
[79] A.U. Hassan, S.H. Sumrra, M. Zubair, G. Mustafa, M.F. Nazar, M.N. Zafar, Structurally modulated D-π-DA (semiconductor) anchoring dyes to enhance the tunable NLO response: a DFT/TDDFT quest for new photovoltaic materials, Struct. Chem. 34 (3) (2023) 1043–1060.
[80] P.O. Andersson, T. Gillbro, L. Ferguson, R.J. Cogdell, Absorption spectral shifts of carotenoids related to medium polarizability, Photochem. Photobiol. 54 (3) (1991) 353–360.
[81] M.I. Khan, Stabilization of betalains: a review, Food Chem. 197 (2016) 1280–1285.
[82] S. Aronoff, The absorption spectra of chlorophyll and related compounds, Chem. Rev. 47 (2) (1950) 175–195.
[83] G. Cinque, R. Croce, R. Bassi, Absorption spectra of chlorophyll a and b in Lhcb protein environment, Photosynth. Res. 64 (2000) 233–242.
[84] C. Anselmi, E. Mosconi, M. Pastore, E. Ronca, F. De Angelis, Adsorption of organic dyes on TiO 2 surfaces in dye-sensitized solar cells: interplay of theory and experiment, Phys. Chem. Chem. Phys. 14 (46) (2012) 15963–15974.
[85] T.-D. Nguyen, Y.-P. Lan, C.-G. Wu, High-efficiency cycloruthenated sensitizers for dye-sensitized solar cells, Inorg. Chem. 57 (3) (2018) 1527–1534.
[86] Z. Li, Q. Li, C. Li, Y. Xie, Panchromatic porphyrin-based dye-sensitized solar cells: from cosensitization to concerted companion dye approaches, Materials Chemistry Frontiers 8 (3) (2024) 652–680.
[87] J.-M. Barichello, Paolo Vesce, Luigi Spadaro, Donatella Citro, Ilaria Matteocci, Fabio Bartolotta, Antonino Di-Carlo, Aldo Calogero, Giuseppe, Bifacial dye-sensitized solar cells for indoor and outdoor renewable energy-based application, J. Mater. Chem. C 12 (7) (2024) 2317–2349.
[88] R. Sasikumar, S. Thirumalaisamy, B. Kim, B. Hwang, Dye-sensitized solar cells: insights and research divergence towards alternatives, Renew. Sustain. Energy Rev. 199 (2024) 114549.
[89] S.N. Tamilselvan, S. Shanmugan, Towards sustainable solar cells: unveiling the latest developments in bio-nano materials for enhanced DSSC efficiency, Clean Energy 8 (3) (2024) 238–257.
[90] A. Kamboj, K. Medha, V. Gupta, S. Jose, Ultraviolet protection of textiles with herbal dyes: a contemporary review, Sustain. Chem. Pharm. 41 (2024) 101689.
[91] S. Kim, T.-G. Hwang, W.-J. Choi, H.-K. Lee, H.-M.-P. Kim, Jong-Mok, J.-P. Kim, Thermally stable and highly soluble UV absorbers for colorless polyimide film: star-shaped hydroxyphenyl benzotriazole with a tailored trade-off between molecular planarity and distortion, Prog. Org. Coat. 191 (2024) 108399.